




The Higgs boson mass as fundamental parameter of the minimal supersymmetric standard model

Rima El-Kosseifi^{1,5}, Jean-Loic Kneur^{2,a}, Gilbert Mourtaka^{2,b} , Dirk Zerwas^{3,4,c}

¹ CPPM, Aix-Marseille Université, CNRS/IN2P3, Marseille, France

² Laboratoire Charles Coulomb (L2C), Université de Montpellier, CNRS, Montpellier, France

³ IJCLab, Université Paris-Saclay, CNRS/IN2P3, Orsay, France

⁴ DMLab, CNRS/IN2P3, Hamburg, Germany

⁵ Present Address: Apneal/Mitral SAS, Charenton-le-Pont, France

Received: 17 February 2022 / Accepted: 11 July 2022 / Published online: 30 July 2022

© The Author(s) 2022

Abstract In the Minimal Supersymmetric Standard Model (MSSM) the mass of the lightest neutral Higgs boson is determined by the supersymmetric parameters. In the m_h MSSM the precisely measured Higgs boson replaces the trilinear coupling A_t as input parameter. Expressions are derived to extract A_t in a semi-analytical form as a function of the light Higgs boson (pole) mass. An algorithm is developed and implemented at two-loop precision, generalizable to higher orders, to perform this inversion consistently. The result of the algorithm, implemented in the SuSpect spectrum calculator, is illustrated on a parameter set compatible with LHC measurements.

1 Introduction

In the Minimal Supersymmetric Standard Model (MSSM) the scalar boson discovered by ATLAS and CMS [1, 2] is identified with the lightest neutral Higgs boson of the model. Its mass has been determined to be 125.10 GeV with a precision of 0.14 GeV when combining the measurements of ATLAS and CMS [3–6].

Given the precision of the measurement it is tempting to express model parameters of the MSSM as a function of this measurement, as it is customarily done for the fermion masses. This choice is also similar to e.g. the almost universally adopted convention of expressing electroweak BSM model parameters as functions of the Z-boson pole mass input, m_Z , after its precise determination at LEP1 in the early 1990s [7]. This procedure was analytically nontrivial beyond tree-level as it necessarily involved the radiative corrections

contributing to the Z-boson pole mass (for the state of the art see [8] and references therein). In the MSSM, the relation of the lightest Higgs boson mass m_h to the basic model parameters is even more involved when including the radiative corrections.

The inversion of relations between parameters of a model and a physical observable is facilitated by approximations which are more easily amenable to such a procedure. In the MSSM this approach has been studied in the gaugino-Higgsino sector [9–11] and in the Higgs sector [11, 12]. By construction the precision of the approach depends on the precision of the approximation which has to be compared to the precision of the experimental measurement. Thus the development of an algorithm to cope with the highest available precision is developed in this paper.

There is a second motivation for the replacement of the model parameter. If a full exploration of the MSSM parameter space is performed, a large fraction of the parameter sets studied will not predict a lightest neutral Higgs boson mass in agreement with the experimental measurement. Using m_h as parameter has the potential to lead to a more efficient exploration of the MSSM.

In the following the MSSM with m_h as parameter is referred to as m_h MSSM to differentiate the model from the standard MSSM. It is well known that m_h depends non-trivially and strongly on the trilinear coupling A_t as well as on the third generation squark sector soft breaking masses via its leading radiative corrections. Because of the $A_t \leftrightarrow m_h$ connection, it is natural to choose to develop the inversion with A_t replaced by m_h as model parameter in the m_h MSSM. The study is carried out within the CP-conserving version of the MSSM where A_t is real-valued, and relies on the fixed-order loop approximations. We will comment on departure from these assumptions towards the end of the paper.

^a e-mail: jean-loic.kneur@umontpellier.fr

^b e-mail: gilbert.mourtaka@umontpellier.fr (corresponding author)

^c e-mail: Dirk.Zerwas@in2p3.fr

Inverting a relationship between two parameters can be performed in multiple ways. A brute force approach would be to calculate m_h as function of all MSSM parameters as well as their SM inputs, taking into account the experimental and systematic errors. This is time consuming and inefficient as in most of the parameter space the predicted m_h is too light with respect to the experimental measurement. Machine Learning algorithms are more efficient but need extensive training and validation. For each update of the calculations the full procedure of determination and validation has to be performed again. For these reasons an algorithmically simple procedure, the fixed point algorithm, is used. It has the advantage that its preparation is analytical work, i.e., an appropriate function has to be derived and the convergence criteria have to be fulfilled. The guiding principle behind this choice is that the additional calculations should add minimal overhead to the calculation of the spectrum.

The paper is organized as follows. In Sect. 2 the basic generic expressions for the scalar Higgs boson masses in the MSSM, including higher order radiative corrections, are recalled and the notations are defined. The MSSM parameter set to serve as test case for our general approach is defined. In Sect. 3 the inversion $A_t(m_h)$ is first illustrated using an analytical approximation at one-loop level, whose purpose is to serve as first guess within a subsequent more elaborate construction. Then the exact full one-loop expression is given together with a description of the strategy for the inversion algorithm, as well as the consistent implementation of the dominant two-loop contributions. In Sect. 4 the full algorithm is assembled by combining the analytical approximation with the full one-loop and dominant two-loop calculations. The results of its application to the parameter set are discussed, as well as possible extensions. We conclude in Sect. 5 and provide technical material in the appendices.

2 Setting up the MSSM Higgs mass

In this section we briefly recall the main content of the fixed-order (diagrammatic) calculation of m_h . Then we define a parameter set to illustrate numerical results.

2.1 Calculation of the Higgs boson mass

In the standard ‘top-down’ procedure one assumes that all the SM and MSSM parameters are taken as input before determining the light (and heavy) CP-even Higgs boson masses through the diagonalization of the corresponding (momentum dependent) squared mass matrix. The latter has the fol-

lowing generic form:

$$\mathcal{M}_s^2(p^2) = \begin{pmatrix} \bar{m}_{11}^2 - \Pi_{11}(p^2) + \frac{t_1}{v_1} \bar{m}_{12}^2 - \Pi_{12}(p^2) & \\ \bar{m}_{12}^2 - \Pi_{12}(p^2) & \bar{m}_{22}^2 - \Pi_{22}(p^2) + \frac{t_2}{v_2} \end{pmatrix} \quad (1)$$

where

$$\bar{m}_{11}^2 = \bar{m}_Z^2 \cos^2 \beta + \bar{m}_A^2 \sin^2 \beta, \quad (2)$$

$$\bar{m}_{22}^2 = \bar{m}_Z^2 \sin^2 \beta + \bar{m}_A^2 \cos^2 \beta, \quad (3)$$

$$\bar{m}_{12}^2 = -\frac{1}{2}(\bar{m}_Z^2 + \bar{m}_A^2) \sin 2\beta. \quad (4)$$

Here \bar{m}_Z^2 and \bar{m}_A^2 denote the running Z-boson and CP-odd Higgs boson squared masses, β the angle defined by $\tan \beta = v_2/v_1$ where v_1, v_2 are the two Higgs vacuum expectation values, and $\Pi_{ij}(p^2)$ and t_i designate respectively the renormalized self-energy and tadpole loop contributions, formally to arbitrary orders in perturbation theory. In practice we rely on the \overline{DR} renormalization scheme. For reviews on radiative corrections to m_h in the MSSM and original references see e.g. [13, 14], and [15] for a recent up-to-date review.

In Eq. (1) the tree-level contributions involve \bar{m}_A evaluated at a given electroweak symmetry breaking (EWSB) scale Q_{EWSB} , and the MSSM parameter $\tan \beta$. If we ignore momentarily the complication that the running parameters in the expressions above have actually a non-trivial implicit dependence on the other MSSM parameters, the ‘tree-level’ masses of the two CP-even MSSM Higgs states and their mixings are described by only these two unknown MSSM parameters as well as \bar{m}_Z .

Beyond the tree-level the squared mass matrix depends on the external squared momentum p^2 through the self-energies, as shown in Eq. (1). The actual pole masses, m_h and m_H , are then obtained by determining the two solutions $p^2 = p_h^2$ and $p^2 = p_H^2$ to the equation

$$\det(p^2 \mathbf{1} - \mathcal{M}_s^2(p^2)) = 0, \quad (5)$$

and taking $m_{h,H} = \sqrt{\text{Re}(p_{h,H}^2)}$. Obviously, the loop contributions in $\mathcal{M}_s^2(p^2)$ depend also on the chosen (\overline{DR}) renormalization scale.

In this paper we focus on the lighter CP-even Higgs with mass m_h . The self-energies and tadpoles contained in $\mathcal{M}_s^2(p^2)$ have been known to one-loop order exactly since the 1990s [16–19], as well as the QCD [20, 21] and other dominant two-loop corrections in the on-shell scheme [22–24] or in the \overline{DR} scheme [25–33]. The (almost) complete two-loop contributions are also available [34–37], as well as the dominant higher order contributions [38–41]. These have

been included in some analyses (see [15] for details). In practice, the determination of the pole mass m_h is achieved by iterating on its implicit expression Eq. (5), until a sufficient accuracy is reached.

Let us now recall some important features of the scalar sector parameter relationship that will be relevant for our construction. Depending on the phenomenological context, \bar{m}_A may be either an input or a derived quantity. In the first case, typical for low-energy model-independent applications, \bar{m}_A can be a direct input at a given EWSB scale Q_{EWSB} , or inferred from the pole mass m_A taken as input. In the second case, typical for top-down approaches, it is obtained from the Supersymmetry (SUSY) soft-breaking running Higgs mass parameters \bar{m}_{H_u} and \bar{m}_{H_d} , evolved by the renormalization group equations (RGE) down to a scale Q_{EWSB} where the EWSB constraints are imposed:

$$\bar{m}_A^2(Q_{EWSB}) = \frac{1}{\cos 2\beta} (\hat{m}_{H_u}^2 - \hat{m}_{H_d}^2) - \bar{m}_Z^2, \tag{6}$$

$$\mu^2(Q_{EWSB}) = \frac{1}{2} \left((\hat{m}_{H_u}^2 \tan \beta - \hat{m}_{H_d}^2 \cot \beta) \times \tan 2\beta - \bar{m}_Z^2 \right). \tag{7}$$

Here μ denotes the running supersymmetric Higgs mixing parameter, and $\hat{m}_{H_i}^2 \equiv \bar{m}_{H_i}^2 - t_i/v_i$.

The self-energies and tadpole loop contributions in Eq. (1) depend implicitly on all MSSM parameters through their sensitivity to the couplings and masses of (s)particles entering the loops. In particular, the dominant radiative correction originates from the top quark mass m_t as well as the stop masses and mixing, $m_{\tilde{t}}$, $X_t \equiv A_t - \mu/\tan \beta$. A further implicit dependence on these parameters occurs when Eqs. (6) and (7) are imposed. This will be instrumental for the identification of the functional dependence of m_h on the trilinear stop coupling A_t , in order to set up an efficient inversion algorithm leading to $A_t(m_h)$, i.e. in the m_h MSSM.

2.2 Stop Cliff

In order to illustrate the general procedure with a concrete example, an MSSM benchmark parameter set is used in the study. The parameters are listed in Table 1.

The EWSB scale is fixed as suggested in [42]. The numerical value chosen is close to the geometric mean of the top squark masses $m_{\tilde{t}_1}$, $m_{\tilde{t}_2}$. In the following we will use as input parameter either A_t in the MSSM or alternatively m_h in the m_h MSSM. Many parameters of the table have little influence on the value of m_h . They are set to values which are sufficiently large to evade the lower bounds on supersymmetric particle masses determined at the LHC [43–47].

The value of M_1 is chosen to obtain a dominantly Bino LSP χ_1^0 . Of the two soft breaking masses $m_{\tilde{q}3_L}$ is much

Table 1 The Stop Cliff set of MSSM parameters is given. The scale dependent parameters are defined at the EWSB scale with the exception of $\tan \beta$ which is defined at the Z boson scale. The resulting masses of the Higgs, lightest stop and LSP are listed as well

EW	2.0 TeV
$m_{H_d}^2$	3.65740418 TeV ²
$m_{H_u}^2$	−0.213361994 TeV ²
sign(μ)	+
A_t	3.610 TeV
$m_{\tilde{t}_R}$	1.27 TeV
$m_{\tilde{q}3_L}$	3 TeV
M_1	300 GeV
M_2	2 TeV
M_3	3 TeV
A_b, A_τ	0 GeV
$\tan \beta$	10
$m_{\tilde{e}_L} = m_{\tilde{\mu}_L} = m_{\tilde{\tau}_L} = m_{\tilde{e}_R} = m_{\tilde{\mu}_R} = m_{\tilde{\tau}_R}$	2 TeV
$m_{\tilde{q}1_L} = m_{\tilde{q}2_L} = m_{\tilde{u}_R} = m_{\tilde{c}_R} = m_{\tilde{d}_R} = m_{\tilde{s}_R} = m_{\tilde{b}_R}$	3 TeV
m_h	125.012 GeV
$m_{\tilde{t}_1}$	1306 GeV
$m_{\tilde{\chi}_1^0}$	294 GeV

greater than $m_{\tilde{t}_R}$, therefore the lightest top squark is essentially of type R . $m_{\tilde{t}_R}$ dominates the determination of its mass as the mixing angle is small. The resulting masses of the lightest top squark and the LSP are shown in Table 1 as well. The top squark mass of 1.3 TeV was chosen to be close to the exclusion bounds determined at the LHC by ATLAS [48] and CMS [49]. We will refer to the benchmark point of Table 1 as the Stop Cliff.

In order to accurately compare the m_h MSSM to the MSSM determination, we have first adjusted A_t such that $m_h(A_t)$ is driven to its experimental value. The resulting m_h values are rounded to MeV. This is two orders of magnitude more precise than the current experimental precision.

3 From the Higgs boson mass to the trilinear stop coupling

The dependence of m_h on A_t is non-trivial. First a simple well-known approximation will be studied, followed by a full one-loop expression derivation. Finally the two-loop contributions will be included.

The strategy to determine $A_t(m_h)$ relies on identifying first the algebraic dominant dependencies on A_t at the given perturbative order or approximation. Then either the approximation is solved for A_t or the resulting equation at given order is transformed into a fixed-point problem. The latter,

via the intrinsically iterative structure of the determination, will account also for the residual non-algebraic dependencies, leading to the exact determination of $A_t(m_h)$.

3.1 Approximate one-loop inversion

Several approximate expressions have been developed in the past for the dominant radiative corrections to m_h in the MSSM, ranging from simple to sophisticated [50–57]. While the latter cannot compete with the full one-loop plus two-loop calculations available nowadays, some of the approximations including dominant two-loop contributions can be rather precise, depending on the considered MSSM parameter range. In our construction there is no need to rely on the most elaborate approximations. The specific expression that we will use is the well-known one originally derived in [53, 54], see also [56], obtained from considering only the dominant top and stop contributions to the one-loop MSSM effective potential, and using renormalization group properties to resum the leading logarithms of decoupled “heavy” stops (relative to $\sim m_t$):

$$m_h^2 = \bar{m}_h^2 + \frac{3\bar{g}_2^2 \bar{m}_t^4}{8\pi^2 \bar{m}_W^2} \left[\ln \left(\frac{M_S^2}{\bar{m}_t^2} \right) + \frac{X_t^2}{M_S^2} - \frac{X_t^4}{12M_S^4} \right], \quad (8)$$

with the noteworthy quartic and quadratic dependencies on the stop mixing parameter,

$$X_t \equiv A_t - \mu \cot \beta. \quad (9)$$

In Eq. (8), \bar{m}_h is the (running) tree-level Higgs mass

$$\bar{m}_h^2 = \frac{1}{2} \left[\bar{m}_Z^2 + \bar{m}_A^2 - \sqrt{(\bar{m}_A^2 - \bar{m}_Z^2)^2 + 4\bar{m}_Z^2 \bar{m}_A^2 \sin^2(2\beta)} \right], \quad (10)$$

\bar{m}_t the running top mass, \bar{g}_2 the running SU(2) gauge coupling, and $\tan \beta$ the running vev ratio, and we define

$$M_S^2 = \sqrt{(\bar{m}_{\bar{q}_{3L}}^2 + (\frac{1}{2} - \frac{2}{3}s_W^2)\bar{m}_Z^2 \cos 2\beta + \bar{m}_t^2)} \cdot \sqrt{(\bar{m}_{\bar{t}_R}^2 + \frac{2}{3}s_W^2 \bar{m}_Z^2 \cos 2\beta + \bar{m}_t^2)} \quad (11)$$

where $\bar{m}_{\bar{q}_{3L}}^2$ and $\bar{m}_{\bar{t}_R}^2$ are the running soft SUSY-breaking parameters of the third generation associated to the left doublet and the stop singlet.

We choose to evaluate all the running quantities in Eq. (8) at the EWSB scale $Q_{EWSB} \simeq (m_{\bar{t}_1} m_{\bar{t}_2})^{1/2}$, including \bar{m}_t . While this choice for \bar{m}_t , and the definition of M_S in Eq. (11), are somewhat at variance with the literature, we emphasize here that we seek a sufficiently accurate but simple expression whose sole purpose is to serve as a first guess for our genuine algorithm, the latter giving consistently a (perturbatively) “exact” $A_t(m_h)$. To put things in perspective, let us enumerate some important features related to Eq. (8), referring to [53–56] for details:

- Strictly speaking, Eq. (8) is valid for large $\tan \beta$, neglecting $\mathcal{O}(g_i^4)$ terms, and in the limit $M_S \gg m_t$ as an expansion in $\frac{|m_t X_t|}{M_S^2}$. In particular, among other necessary steps [53] in the derivation of Eq. (8) from the MSSM effective potential, the X_t^4 term arises only after expanding to second order in X_t^2 the terms with logarithmic dependence in the stop masses, $\ln m_{\bar{t}_i}^2 \simeq \ln(M_S^2 \pm \bar{m}_t X_t)$ (in the limit $M_S \simeq \sqrt{m_{\bar{q}_{3L}}^2 + \bar{m}_t^2} \simeq \sqrt{m_{\bar{t}_R}^2 + \bar{m}_t^2}$). This approximation was thus a priori expected to be valid only for rather moderate $|X_t/M_S|$, large $\tan \beta$ and for $m_A \gg m_Z$, but turned out to be reasonably good in an extended range.
- In [53–56], the D -terms $\propto m_Z$ in Eq. (11) were accordingly neglected, moreover, universal soft masses, $m_{\bar{q}_{3L}} = m_{\bar{t}_R} \simeq M_{susy}$, were also assumed for simplicity. Actually in the effective field theory (EFT) framework appropriate to derive Eq. (8), M_S is not very precisely defined as long as it is identified as the scale at which the top squarks are decoupled, and the matching to the EFT is done: M_S is assumed in the literature to be of order the average stop masses. In a more refined treatment (or to account for $m_{\bar{t}_1} \ll m_{\bar{t}_2}$) one would need to decouple the two stop masses *separately*, which is beyond the scope of the approximation Eq. (8). Our slightly different definition in Eq. (11) makes minor differences, the important practical feature for our purpose being that M_S in Eq. (11) does not involve an extra dependence on X_t .
- The scale Q_t at which the running top mass $\bar{m}_t(Q_t)$ is evaluated in Eq. (8) is quite relevant due to the \bar{m}_t^4 dependence. While the EFT one-loop calculation in [53, 54] involves $\bar{m}_t(m_t)$, in [55] it was shown that the leading (EFT) two-loop contributions are essentially absorbed by the one-loop expression Eq. (8), if setting $\bar{m}_t(Q_t \equiv (\bar{m}_t M_S)^{1/2})$ and $\bar{m}_t(Q_t \equiv M_S)$, respectively for the term $\sim \ln M_S^2/\bar{m}_t^2$ and mixing terms $\sim \bar{m}_t X_t$. Given that we do not seek the best possible approximation, the choice of a (unique) EWSB scale $Q_{EWSB} \simeq (m_{\bar{t}_1} m_{\bar{t}_2})^{1/2} \sim M_S$ for all running parameters (or any fixed scale sufficiently close to the latter, as often conveniently chosen in Suspect and similar codes [58]) appears to be a reasonable compromise.

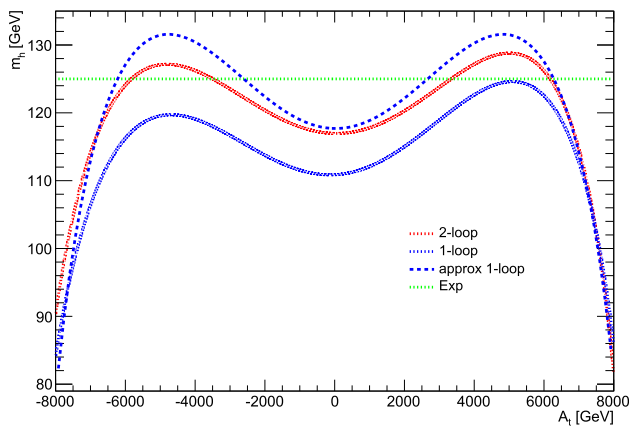


Fig. 1 The prediction of m_h at one- and two-loop precision as well as for the approximate one-loop is shown as function of A_t together with the measured mass

- Equation (8) can also be derived from the diagrammatically obtained $\Pi_{ij}(0)$ self-energies and t_i tadpoles, provided one carefully identifies [56] approximations at the same level as described above.

There exists several refinements of Eq. (8), e.g. including sbottom [55], stau and QCD leading effects [57]. In the following we stick to Eq. (8), referring to it as *approximate* one-loop whose simplicity is important for our construction, as explained next.

In order to determine A_t as a function of the “physical” mass m_h , Eq. (8) is solved as being a quadratic equation in X_t^2 .

The procedure captures an essential feature of the inversion for A_t : in principle there are two X_t^2 solutions which, when real-valued and positive, lead to up to four different A_t solutions. This well-known feature is illustrated in Fig. 1 where we show the m_h prediction for the full one-loop, two-loop and the approximate one-loop calculations. For the $m_h(A_t)$ full one-loop and two-loop results, A_t was varied and for each A_t the EWSB minimisation was performed to derive the running mass of the CP-odd Higgs boson and the μ parameter. All other parameters were fixed to their cliff point values. For the approximate one-loop, the coefficients of Eq. (8) were calculated for the cliff point, thus fixing \bar{m}_A^2 and μ and varying only A_t in the square root of Eq. (8) shown in the figure. For the measured Higgs boson there are four intersections with the prediction. The third intersection (from left to right) with the two-loop prediction is consistent with the A_t cliff point value of 3.61 TeV.

We turn now to the inverse approach of determining A_t from Eq. (8) when the measured m_h is taken as input. The A_t determination is illustrated in Table 2. Four solutions are determined for A_t as expected. The third solution s3 corresponds to the nominal solution: the cliff point. In each one

Table 2 The result of the A_t determination from m_h using Eq. (8) is shown. s3 corresponds to the nominal solution: the cliff point

	A_t [TeV]	
s1	A_t [TeV]	−5.44
s2	A_t [TeV]	−3.61
s3	A_t [TeV]	2.87
s4	A_t [TeV]	6.36

of the solutions \bar{m}_A^2 and μ are those corresponding to the intersection of the two-loop Higgs mass with the measured m_h .

For the nominal A_t in s3 Eq. (8) leads to a Higgs mass larger than the two-loop Higgs mass prediction (see Fig. 1). This is compensated by an A_t value smaller than the nominal one: 2.87 TeV instead of 3.61 TeV. The use of the measured m_h in the calculation therefore inevitably leads to a shift in A_t . Its calculated value is within 25% of the nominal value, a clear improvement compared to a blind guess. At the same time, it clearly illustrates that an accurate $A_t(m_h)$ determination requires a more elaborate construction as compared to Eq. (8), which we will describe next.

3.2 Full one-loop: the HiggsMolar function

For the full one-loop inversion the starting point is the (formally exact) Eq. (5) which we rewrite here as an essentially quadratic equation in the CP-even Higgs squared masses,

$$\begin{aligned}
 m_{h,H}^4 - m_{h,H}^2 \left((\mathcal{M}_s^2)_{11}(p^2) + (\mathcal{M}_s^2)_{22}(p^2) \right) \\
 + (\mathcal{M}_s^2)_{11}(p^2)(\mathcal{M}_s^2)_{22}(p^2) \\
 - \left((\mathcal{M}_s^2)_{12}(p^2) \right)^2 \Big|_{p^2=m_{h,H}^2} = 0,
 \end{aligned} \tag{12}$$

of which m_h^2 corresponds to the lighter mass solution. Here $(\mathcal{M}_s^2)_{ij}(p^2)$ denotes the *real* parts of the matrix element, and the solutions $p^2 = m_{h,H}^2$ are real-valued.¹ The $(\mathcal{M}_s^2)_{ij}(p^2)$'s extracted from Eq. (1) include perturbatively complete loop corrections where the full one-loop Higgs boson self-energies, Π_{ij} , and tadpoles t_i are taken from [19]. In the $\overline{\text{DR}}$ scheme these expressions include contributions from all (s)particles (running) masses, resulting in a highly nonlinear dependence on A_t from the stop sector. In particular the finite part of the one-loop scalar function A_0 , occurring in the tadpoles and self-energies, has a rather involved A_t

¹ Since the matrix elements of $(\mathcal{M}_s^2)(p^2)$ develop imaginary parts, the squared pole masses are, strictly speaking, given by the real parts of the two solutions of Eq. (5). In practice, though, neglecting the imaginary parts in the equation itself is a very good approximation for m_h , since the induced relative error on its estimate (of order $\frac{\Gamma_h}{m_h}$ with Γ_h the total width), is negligibly small compared to other (higher order) theoretical uncertainties.

dependence when its argument is the stop mass:

$$A_0(m_{\tilde{t}_i}) = m_{\tilde{t}_i}^2 \left(1 - \ln \left(\frac{m_{\tilde{t}_i}^2}{Q^2} \right) \right) \tag{13}$$

where Q is the $\overline{\text{DR}}$ -scheme renormalization scale, and where from the stop sector diagonalization, the $\overline{\text{DR}}$ -scheme running stop masses can be written as

$$m_{\tilde{t}_{1,2}}^2 = \frac{1}{2} \left(M^2 \mp \sqrt{a_s A_t^2 + b_s A_t + c_s} \right), \tag{14}$$

where

$$\begin{aligned} M^2 &= m_{\tilde{q}_{3L}}^2 + m_{\tilde{t}_R}^2 + 2m_t^2 + \frac{1}{2}m_Z^2 \cos 2\beta, \\ a_s &= 4m_t^2, \\ b_s &= -8m_t^2 \mu \cot \beta, \\ c_s &= \left(m_{\tilde{q}_{3L}}^2 - m_{\tilde{t}_R}^2 + \left(\frac{1}{2} - \frac{4}{3}s_W^2 \right) m_Z^2 \cos 2\beta \right)^2 \\ &\quad + 4m_t^2 \mu^2 \cot^2 \beta, \end{aligned} \tag{15}$$

are A_t independent.² The strategy is to rewrite Eq. (12) as an equation for A_t by extracting from Eq. (1) the explicit polynomial A_t dependencies or “power counting” within each Π_{ij} and t_i . On close inspection of the various contributions in e.g. [19] we identify:

1. terms depending linearly on A_t (with coefficients identified by a superscript ‘1’), originating from the $s_k\tilde{t}_i\tilde{t}_j$ couplings, $g_{s_2\tilde{t}_1\tilde{t}_1}, g_{s_2\tilde{t}_2\tilde{t}_2}, g_{s_2\tilde{t}_1\tilde{t}_2}$ which are given by

$$\begin{aligned} g_{s_2\tilde{t}_1\tilde{t}_1} &= c_t^2 g_{s_2\tilde{t}_L\tilde{t}_L} + 2c_t s_t g_{s_2\tilde{t}_L\tilde{t}_R} + s_t^2 g_{s_2\tilde{t}_R\tilde{t}_R}, \\ g_{s_2\tilde{t}_2\tilde{t}_2} &= s_t^2 g_{s_2\tilde{t}_L\tilde{t}_L} - 2c_t s_t g_{s_2\tilde{t}_L\tilde{t}_R} + c_t^2 g_{s_2\tilde{t}_R\tilde{t}_R}, \\ g_{s_2\tilde{t}_1\tilde{t}_2} &= s_t c_t (g_{s_2\tilde{t}_R\tilde{t}_R} - g_{s_2\tilde{t}_L\tilde{t}_L}) + (c_t^2 - s_t^2) g_{s_2\tilde{t}_L\tilde{t}_R}, \\ g_{s_2\tilde{t}_L\tilde{t}_R} &= \frac{y_t}{\sqrt{2}} A_t, \end{aligned} \tag{16}$$

with y_t the top quark Yukawa coupling, $s_t \equiv \sin \tilde{\theta}_t$, $c_t \equiv \cos \tilde{\theta}_t$, where $\tilde{\theta}_t$ denotes the stop mixing angle, \tilde{t}_1, \tilde{t}_2 are the stop mass eigenstates, \tilde{t}_L, \tilde{t}_R the gauge eigenstates, and s_k are the neutral scalar states in the basis corresponding to Eq. (1). Note that $g_{s_2\tilde{t}_R\tilde{t}_R}, g_{s_2\tilde{t}_L\tilde{t}_L}$ do not depend explicitly on A_t , their expressions can be found e.g. in [19] (denoted by $\lambda_{s_2\tilde{u}_{L,R}\tilde{u}_{L,R}}, \lambda_{s_2\tilde{u}_L\tilde{u}_R}$ therein).

² Note that M^2 gives the accurate combination entering the exact one-loop expressions considered here. M_S^2 in Eq. (11) is in general obviously unequal to $\frac{1}{2}M^2$, unless $m_{\tilde{q}_{3L}}^2 = m_{\tilde{t}_R}^2$ and the D-terms are neglected. We use it in Eq. (8) as a practical approximation for m_h .

2. terms depending quadratically on A_t (with coefficients identified by a superscript ‘2’), originating from the $g_{s_2\tilde{t}_i\tilde{t}_i}^2$ that appear solely in $\Pi_{22}(p^2)$;
3. terms depending on $\sqrt{a_s A_t^2 + b_s A_t + c_s}$ (with coefficients identified by ‘s’) originating from the $m_{\tilde{t}_i}^2$ in $A_0(m_{\tilde{t}_i})$;
4. a term containing $A_t \cdot \sqrt{a_s A_t^2 + b_s A_t + c_s}$ (with coefficient identified by ‘1s’) resulting from the occurrence of the product $g_{s_2\tilde{t}_i\tilde{t}_i} \times A_0(m_{\tilde{t}_i})$ appearing solely in t_2 ;
5. finally all remnant contributions with no (explicit) dependence or with logarithmic dependence on A_t , are identified by a ‘0’ superscript. It is an important part of our strategy that in our A_t -power counting any “logarithmic” dependence $\sim \ln(M^2 \mp \sqrt{a_s A_t^2 + \dots})$ on A_t (such as in the second term of Eq. (13)), and in the one-loop scalar function B_0), as well as the other algebraic dependence on A_t in B_0 , are incorporated exactly as they stand within the coefficients of the above listed relevant A_t powers. In the following we dub these dependencies “residual”. The dependence of the stop mixing angle $\tilde{\theta}_t$ on A_t is also treated as residual, since it enters in Eq. (16) through c_t and s_t that remain obviously bounded functions of A_t .

According to the previous A_t power counting, within the relevant (one-loop) Π_{ij} and t_i individual contributions, there are no higher degree monomials in A_t than the A_t^k identified above with $k \leq 2$. This gives the following formal decomposition of the tadpoles and self-energies:

$$\begin{aligned} \frac{t_1}{v_1} &= t_1^{(s)} \sqrt{a_s A_t^2 + b_s A_t + c_s} + t_1^{(0)} \\ \frac{t_2}{v_2} &= t_2^{(1s)} A_t \sqrt{a_s A_t^2 + b_s A_t + c_s} + t_2^{(1)} A_t \\ &\quad + t_2^{(s)} \sqrt{a_s A_t^2 + b_s A_t + c_s} + t_2^{(0)} \\ \Pi_{11} &= \pi_{11}^{(s)} \sqrt{a_s A_t^2 + b_s A_t + c_s} + \pi_{11}^{(0)} \\ \Pi_{12} &= \pi_{12}^{(1)} A_t + \pi_{12}^{(0)} \\ \Pi_{22} &= \pi_{22}^{(2)} A_t^2 + \pi_{22}^{(1)} A_t \\ &\quad + \pi_{22}^{(s)} \sqrt{a_s A_t^2 + b_s A_t + c_s} + \pi_{22}^{(0)}. \end{aligned} \tag{17}$$

Equation (17) is simply a convenient rewriting of already available exact one-loop expressions, no contributions are ignored. Using Eq. (17) to display the algebraic dependence on A_t in Eq. (12), the following molar-shaped function $\text{HiggsMolar}(A_t)$, which should consistently vanish for any A_t solution, is obtained:

$$\begin{aligned} \text{HiggsMolar}(A_t) &= C_3 A_t^3 + C_2 A_t^2 + C_1 A_t + C_0 \\ &\quad + (R_2 A_t^2 + R_1 A_t + R_0) \sqrt{a_s A_t^2 + b_s A_t + c_s} = 0. \end{aligned} \tag{18}$$

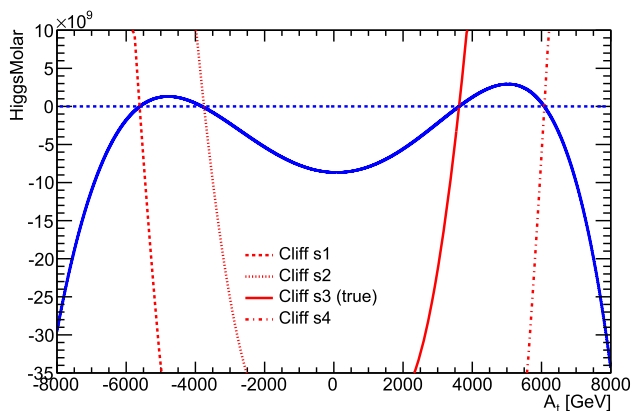


Fig. 2 The distribution of the HiggsMolar is shown as function of A_t : calculating the coefficients of Eq. (18) for each A_t (solid blue curve); fixing the coefficients of Eq. (18) at the four A_t solutions (red curves). For the four solutions, given by the intersections with the dotted blue line, only the A_t range around the solution is shown by the red curves

The HiggsMolar is shown as function of A_t in Fig. 2. For each A_t the coefficients are recalculated. The four other curves show the behavior of the function if the coefficients determined at the intersections of the HiggsMolar with the line HiggsMolar = 0 are used in the vicinity of the intersections. The curves illustrate the variation of the coefficients.

This equation can in principle be used separately either for the lighter or for the heavier CP-even Higgs masses, as clear from Eq. (12). Hereafter we are only considering the lighter Higgs mass at ~ 125 GeV as input. The C_i and R_i coefficients are easily identified upon use of Eqs. (1), (12) and (17). They contain all the residual A_t dependencies quoted above, neglecting all imaginary parts as justified in footnote 1.

The cubic term results from the product $(t_1 - \Pi_{11}) \times t_2$ present in $(\mathcal{M}_s^2)_{11}(\mathcal{M}_s^2)_{22}$, with a coefficient C_3 given by

$$C_3 = 4\bar{m}_t^2 (t_1^{(s)} - \pi_{11}^{(s)})t_2^{(1s)}. \tag{19}$$

In particular, in contrast with Eq. (8) and unless performing in Eq. (18) an expansion in X_t , explicit $X_t^4 \sim A_t^4$ terms cannot occur within the exact Eq. (12) as the equation does not involve squares of terms of the type ‘2’ or ‘1s’.

The general form of the other C_i and R_i coefficients is given in Appendix A. These coefficients have a more involved dependence on (differences of) the quantities $\pi_{ij}^{(0,s,1,2)}$ and $t_i^{(0,s,1,1s)}$ entering Eq. (17). The relevant one-loop expressions of the latter are also given in Appendix A. They allow to track the residual dependence on A_t and the absence of some finite combinations in relation to the expected cancellation of the quadratic divergences in softly-broken SUSY. The full one-loop explicit dependence on A_t is thus included in Eq. (18). A further implicit dependence on A_t will originate

from the two EWSB conditions Eqs. (6), (7) when imposed beyond the tree-level, due to the presence of \bar{m}_A^2 as well as μ in the C_i and R_i coefficients. In particular, the t_2 -tadpole dependence in \bar{m}_A^2 will induce, through the term $\bar{m}_{11}^2 \times t_2$ appearing in the cross-product $(\mathcal{M}_s^2)_{11}(\mathcal{M}_s^2)_{22}$ in Eq. (12), an effectively *quartic* dependence on A_t for large A_t , not explicit in Eq. (18). This entails solving simultaneously Eq. (18) and the EWSB constraints Eqs. (6) and (7), which we will perform numerically in a consistent way as described in Sect. 4.1. Other implicit dependencies on A_t are discussed in Sect. 3.5. Hereafter we ignore momentarily these issues and focus solely on the resolution of Eq. (18).

3.3 Full one-loop inversion: the fixed point algorithm

To solve Eq. (18) for A_t , a fixed point iterative method is used. For this purpose we define

$$C_{FP}(A_t) = -\frac{1}{C_3} \left(C_2 A_t^2 + C_1 A_t + C_0 + (R_2 A_t^2 + R_1 A_t + R_0) \sqrt{a_s A_t^2 + b_s A_t + c_s} \right), \tag{20}$$

and rewrite Eq. (18) as

$$A_t = \sqrt[3]{C_{FP}(A_t)}. \tag{21}$$

It is then clear that finding all the real-valued solutions of Eq. (18) is equivalent to determining all the fixed points $A_t = A_t^{FP}$, satisfying $L_{FP}(A_t^{FP}) = A_t^{FP}$, of the function L_{FP} defined by

$$L_{FP}(A_t) \equiv \sqrt[3]{C_{FP}(A_t)}, \tag{22}$$

with only *real-valued* cubic roots allowed.

To determine the fixed points one starts from a guess value $A_{t,0} = A_t^{Guess}$ and studies the convergence of the sequence $A_{t,i+1} = L_{FP}(A_{t,i})$. The iterations return unambiguously real-valued A_t as a consequence of the definition of L_{FP} , Eq. (22). As we will specify in more detail in Sect. 4, appropriate A_t -guess values, not too far from the exact solutions, are those obtained from our approximate one-loop Eq. (8) that already captures the multi-solution structure. However, even if starting relatively close to the exact solutions, the method will catch only the *attractive* fixed points and can thus miss some, otherwise acceptable, A_t solutions.

One expects typically four distinct solutions as illustrated in Fig. 3 for the stop cliff benchmark: The functions $C_{FP}(A_t)$ and $L_{FP}(A_t)$, in blue, intersect the dotted blue lines at the fixed points of these functions, corresponding to the four A_t solutions that are consistent with $m_h = 125$ GeV. For the blue curve the coefficients C_i and R_i of the two fixed-point functions were recalculated at each A_t . For the four red curves

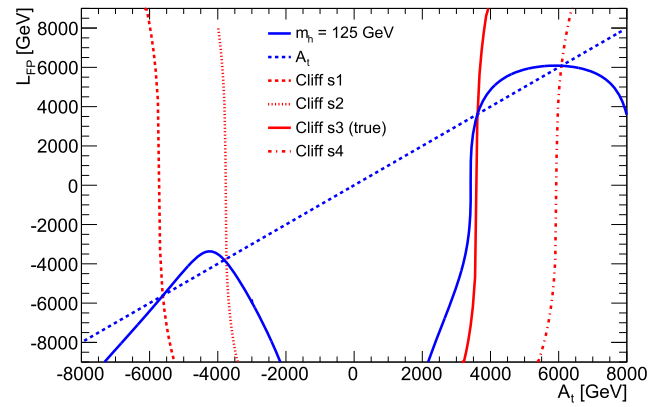
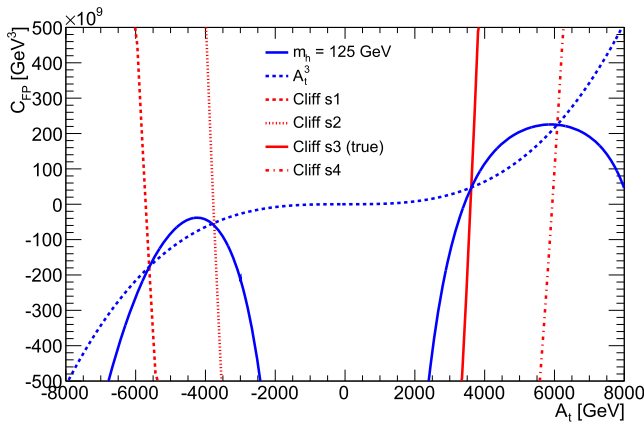


Fig. 3 The distributions of the functions C_{FP} and L_{FP} are shown as function of A_t : calculating the coefficients of Eq. (18) for each A_t (solid blue curve); fixing the coefficients of Eq. (18) at the four A_t solutions

(red curves). For the four solutions, given by the intersections with the dotted blue line, only the A_t range around the solution is shown by the red curves

these coefficients are frozen at their values calculated at the intersection of the blue curve with the blue dotted line, for A_t varying in the vicinity of the intersection.

The dotted blue line on Fig. 3-right being the bisector, it follows that the slope of L_{FP} at its fixed points is alternatively greater or smaller than one. We label the solutions $s1, s2, s3, s4$ ordered in ascending in A_t . Given that L_{FP} takes negative values for very large $|A_t|$, the slopes of L_{FP} at $s1$ and $s3$ are necessarily greater than one and those at $s2$ and $s4$ less than one. $s1$ and $s3$ are thus *repulsive* fixed points. In contrast, $s2$ and $s4$ will be either *attractive* if the slope is between -1 and 1 , or *alternating/repulsive* if the slope is less than -1 . The slope at $s2$ is typically less than zero due to the strong variation of L_{FP} in the vicinity of $|A_t| \sim 0$. It follows that the iterative procedure on L_{FP} as described above will always miss solutions $s1$ and $s3$ while capturing at best two solutions, namely $s2$ and $s4$, provided furthermore the initial guess values A_t^{Guess} close enough to $s2$ and $s4$ to feel their attracting character. If a guess point is chosen anywhere above $s3$ the iterations will repel it from $s3$ and converge to $s4$. If chosen below $s1$ it will be repelled to the left and the procedure will never converge. Finally, if chosen between $s1$ and $s3$ then, depending on the behaviour around $s2$, the convergence to $s4$ (and occasionally to $s2$ if its slope is greater than -1) may or may not occur.

In order to ensure convergence and be able to capture all solutions, we consider a generalized family $L_{FP\tau}$ of functions parametrized by $\tau \neq 0$ as follows:

$$L_{FP\tau}(A_t) = \frac{1}{\tau}(L_{FP}(A_t) - A_t) + A_t. \tag{23}$$

Any fixed point of L_{FP} is also a fixed point of $L_{FP\tau}$ and vice versa, for any value of τ .

Moreover from

$$L'_{FP\tau}(A_t) = 1 + \frac{L'_{FP}(A_t) - 1}{\tau}, \tag{24}$$

follows that one can always choose τ in such a way that $L'_{FP\tau}(A_t^{FP})$ lies in the interval $[-1, 1]$ for any given value of $L'_{FP}(A_t^{FP})$. Thus the advantage of $L_{FP\tau}$ is that all fixed points of L_{FP} can be made *attractive* with respect to $L_{FP\tau}$ for appropriately chosen values of τ . In this case an iteration over the sequence $A_{t,i+1} = L_{FP\tau}(A_{t,i})$ is guaranteed to converge on A_t^{FP} , at least when the initial guess values are not too far from the solution. However, A_t^{FP} is not known in advance, even less $L'_{FP}(A_t^{FP})$. Without this knowledge, a rough strategy to converge on a given solution could be to choose:

- $\tau \gtrsim 1$ for $s4$
- $\tau \ll -1$ for $s1, s3$
- $\tau \gg 1$ for $s2$.

Actually one can do better by determining optimal values of τ from the knowledge of the local variation of L_{FP} during the iterative procedure. A numerical estimate $\Delta L_{FP}/\Delta A_t$ of the first derivative of L_{FP} with respect to A_t can in principle be calculated at any given step during the iterations on A_t at moderate computational cost. Then choosing the τ parameter as follows

$$\begin{aligned} \frac{\Delta L_{FP}}{\Delta A_t} - 1 < 0 : \tau &= + \left| \frac{\Delta L_{FP}}{\Delta A_t} - 1 \right|, \\ \frac{\Delta L_{FP}}{\Delta A_t} - 1 > 0 : \tau &= - \left| \frac{\Delta L_{FP}}{\Delta A_t} - 1 \right|, \end{aligned} \tag{25}$$

ensures that an estimate of the derivative of $L_{FP\tau}$ is close to zero, cf. Eq. (24). Since this estimate is in practice not at

the fixed point, Eq. (25) is not sufficient to guarantee convergence. However, it approximates a necessary condition, fulfilling a convergence criterion discussed in Appendix B, see Eq. (B.17). This allows to make any fixed point attractive, provided initial guess values are not too far from that fixed point. A simple and efficient algorithm will be implemented along these lines, as described in Sect. 4.

3.4 Dominant two-loop inversion

The extension of the above exact one-loop method to the two-loop contributions is rather straightforward. The latter corrections depend dominantly on the strong, weak and third generation Yukawa couplings y_i , leading to terms of $\mathcal{O}(\alpha_{s,i}) \times \mathcal{O}(\text{One-loop})$, where $\alpha_i \equiv y_i^2/(4\pi)$. In the standard fixed-order (diagrammatic) m_h calculations, $\Pi_{ij}^{(2-loop)}$ and $t_i^{(2-loop)}$ contributions are added to the \mathcal{M}_s^2 matrix elements which enter the squared Higgs boson mass equation shown in Eq. (12).

Due to the extra loop suppression factor, at any scale relevant for the MSSM spectrum calculation where either $\alpha_s(Q)$ or $\alpha_t(Q)$ remain moderate, the two-loop contributions are a moderate correction relative to the one-loop contributions (even if including those is obviously very relevant for a more precise comparison between the MSSM prediction and the measured m_h value. For instance typically for the benchmark cliff point, restricting to exact one-loop would give $m_h \sim 118$ GeV instead of ~ 125 GeV as in Table 1.) Thus, for the $A_t(m_h)$ inversion, rather than trying to extract specific quite involved A_t dependencies from the $\Pi_{ij}^{(2-loop)}$ and $t_i^{(2-loop)}$ contributions, the latter are incorporated just as they contribute to Eq. (1): more precisely, within the above algorithm the available two-loop contributions are formally treated as if they were independent of A_t , therefore concretely incorporated as additional contributions to either $t_i^{(0)}$ or $\pi_{ij}^{(0)}$ in Eq. (17):

$$t_i^{(0)} \rightarrow t_i^{(0)} + t_i^{(2-loop)}, \quad \pi_{ij}^{(0)} \rightarrow \pi_{ij}^{(0)} + \Pi_{ij}^{(2-loop)}. \quad (26)$$

This is then corrected iteratively for the true A_t dependence. The seven coefficients entering the HiggsMolar(A_t) function of Eq. (18) can now be computed incorporating consistently two-loop contributions.

3.5 Including higher orders and refinements

At this stage the inversion is formally ‘exact’ at the considered (perturbative) level of theoretical precision taken for the t_i tadpoles and self-energy contributions Π_{ij} , namely full one-loop and only the dominant two-loop contributions. It is a straightforward matter to incorporate either more complete two-loop and/or higher (3-loop) contributions, by con-

sidering those contributions similarly A_t independent, since their actual A_t dependence, independent of its complexity, is screened by tiny perturbative expansion coefficients. As long as higher order corrections are obtained diagrammatically in the form of self-energy or tadpole contributions, these could be included explicitly by adding them to the $t_i^{(0)}$ and $\pi_{ij}^{(0)}$ contributions.

It is well known that sizeable theoretical uncertainties in m_h determinations (customarily taken as $\sim \pm 2 - 3$ GeV in phenomenological analyses) are due to presently unknown higher order contributions, discrepancies between different renormalization schemes, etc (see e.g. [33,59], or for more recent analyses [60,61], as well as the recent updated discussion in [15]). Given these uncertainties, one might question the importance of devising a very accurate inversion procedure. The answer is obvious: not to introduce artificially further uncertainties in the determination of $A_t(m_h)$ than there are from a given content of higher order contributions included in the standard m_h determination. Related to this, there remains one subtlety to consider: Even at one-loop level, there are extra implicit A_t dependencies that would not be accounted for by the previous algorithm, if one relied solely on the procedure leading to Eq. (18). Indeed, the self-energies and tadpoles also depend typically on SM-like gauge and Yukawa couplings, as well as other running $\overline{\text{DR}}$ parameters (s_W, m_W), which are affected by threshold corrections, depending themselves on the MSSM parameters, therefore depending on A_t in a highly nontrivial way in this case. While all these threshold corrections give contributions that are formally of higher (at least two-loop) order *within* the loop self-energy and tadpole expressions, they can induce a numerical inconsistency bias if not incorporated in the inversion, slightly shifting the resulting $A_t(m_h)$ with respect to its actual ‘reference’ value in a standard top-down calculation. This, as well as the other residual or implicit dependencies on A_t already mentioned in Sect. 3.2, are, however, consistently taken into account in the full algorithm as we explain next.

4 The full inversion algorithm

The algorithm has been implemented in SuSpect3 [62,63]. SuSpect3 is a public spectrum calculator for multiple supersymmetric models that includes, within Eq. (1) for m_h , the $\overline{\text{DR}}$ radiative corrections at full one-loop and dominant two-loop orders (involving for the latter the QCD and third family Yukawa contributions, but at vanishing p^2). Other MSSM spectrum calculators are, non-exhaustively, SOFT-SUSY [64], SPHENO [65–67], FeynHiggs [22,57,68,69], and FlexibleSUSY [70]. Note that on top of fixed-order calculations including some contributions beyond the above mentioned two-loop order, some of these codes (FeynHiggs, SPHENO, FlexibleSUSY) also include resummations of

large logarithms in an EFT approach for the Higgs mass calculations, thus with an a priori increased precision for large soft-supersymmetry breaking mass scenarios.

Before describing the full inversion algorithm, let us first briefly recall the procedure to determine the spectrum in the MSSM. This involves solving the RGE to evolve the parameters between the EWSB scale (Q_{EWSB}) and the scale given by the mass of the Z boson (m_Z), as well as solving the EWSB equations Eqs. (6) and (7) at Q_{EWSB} . Radiative corrections to the supersymmetric particle and Higgs boson masses are calculated at Q_{EWSB} . Supersymmetric radiative corrections to Standard Model parameters, the most important in the present study being the top Yukawa coupling, are calculated at m_Z .

For EWSB three variants have been implemented. If $\overline{m}_{H_d}^2$, $\overline{m}_{H_u}^2$ and the sign of μ are given as input, the running mass squared \overline{m}_A^2 and the Higgs mass parameter μ are calculated. Alternatively μ and either the pole mass m_A or the tree-level running mass squared \overline{m}_A^2 can be given to calculate $\overline{m}_{H_d}^2$, $\overline{m}_{H_u}^2$.

Both the RGE evolution and the EWSB calculations are implemented as iterations. The convergence is tested on the stability of \overline{m}_A^2 or $\overline{m}_{H_u}^2$ between successive iterations. The choice depends on the input parameter set chosen.

We recall that for a precise calculation of the MSSM spectrum in the standard top-down approach, it is essential that some of the relevant running parameters at a given scale, and consequently the physical (pole) masses, are calculated iteratively, as these parameters are nontrivially modified by radiative corrections, which in turn depend on potentially all MSSM parameters.³ There is also an iteration between the EWSB and m_Z scales, since important radiative corrections, depending themselves on the MSSM spectrum, are incorporated to extract the $\overline{\text{DR}}$ -scheme gauge and Yukawa couplings upon matching their experimentally measured values. The convergence criterion for the RGE iteration depends on the choice for the EWSB parameters.

4.1 Algorithm

In the m_h MSSM the $A_t(m_h)$ determination algorithm extends the previously described calculation of the relevant EWSB parameters of the MSSM in SuSpect3. The determination of A_t has been added to this already necessarily iterative structure as the determination of an additional parameter. The algorithm to determine A_t is independent of the parameter input choice. In the following the numerical examples are given for an input of $\overline{m}_{H_d}^2$, $\overline{m}_{H_u}^2$ and the sign of μ . The calculation starts with the RGE evolution from the Z boson scale

to a high scale. A_t is initialized arbitrarily to a fixed value (10 GeV) as the parameter will be determined after the RGE evolution to Q_{EWSB} . The procedure is similar to the initialization of μ .

First the MSSM EWSB calculations are performed, i.e., μ and \overline{m}_A^2 are determined, and then A_t is determined. This procedure is repeated until convergence is reached according to the MSSM criteria, i.e., μ is stable and therefore \overline{m}_A^2 is stable as well.

At the first and second RGE iteration the approximate one-loop Eq. (8) with the measured m_h as input is solved to extract a new A_t as explained in Sect. 3.1. Taking into account the newly determined A_t , the RGE evolution to the Z mass scale is performed. Radiative corrections are calculated, in particular to the top Yukawa terms. The parameters are then RGE evolved to the high scale. The second RGE iteration therefore starts at the high scale with the A_t value derived from the approximate one-loop algorithm in the first iteration.

For the cliff point, Table 2 shows that the correct A_t is within 25% of the calculated value. The use of Eq. (8) is preferred over the fixed point algorithm as the radiative corrections used depend on $y_t \cdot \mu$. This allows to stabilize quickly y_t with an approximate A_t at low computational cost. Using the full radiative calculations at this stage would lead to longer iterations as the variations of both μ and A_t take longer to stabilize.

For the third and all following RGE iterations the full radiative calculations are used for EWSB, combined with the fixed point algorithm described in Sects. 3.3 and 3.4 to determine A_t . For each new A_t , obtained from $L_{\text{FP}\tau}$, Eq. (23), the tree-level stop sector and the Higgs sector including radiative corrections are recalculated. This has the advantage that not only the leading terms of $L_{\text{FP}\tau}$, Eq. (22), are taken into account, but also both the residual and implicit A_t dependencies in the coefficients C_i and R_i , as explained previously. The recalculation of the stop sector and the Higgs sector for each iteration brings the function from the red curves closer to the blue (nominal) curves in Figs. 2 and 3.

The convergence depends on the τ parameter. When the full radiative corrections are used in the algorithm, an estimate $\Delta L_{\text{FP}}/\Delta A_t$ of the first derivative of L_{FP} with respect to A_t is calculated numerically at the end of the iteration on A_t . The iterations are stopped when the relative change of A_t between the last and the current value is smaller than a threshold. Numerical values are given below. The τ parameter is then adjusted according to Eq. (25) which is used in the next determination of A_t .

4.2 Proof of concept

As proof of concept the calculation is performed for all four possible solutions using the full algorithm. The A_t is first determined via the approximate one-loop calculation for the

³ In particular for determining μ from Eq. (7) since the right hand side depends itself implicitly on μ from the tadpole contributions.

Table 3 The result of the Higgs inversion algorithm is shown for the stop cliff. The true point is s3. As a cross check the m_h values shown are the result of the standard $m_h(A_t)$ calculation with the A_t obtained from the input m_h parameter

Stop cliff	s1	s2	s3	s4
A_t [GeV]	-5617.3	-3796.1	3609.7	6082.5
m_h [GeV]	125.012	125.012	125.012	125.012

first two RGE iterations and then the fixed point algorithm is used for all following iterations. A_t is refined at each step. To converge on the spectrum calculation the RGE iterations are stopped once \bar{m}_A is stabilized to the permil level. The EWSB iterations are stopped when μ has converged at permil level. The iterations on A_t are run with a convergence criterion of permil.

The results of the full algorithm are shown in Table 3. Four solutions are obtained as expected. The calculation of A_t and the calculated m_h are in excellent agreement with the expected values.

In point s3 the deviation of the calculated A_t value from the expected value in Table 1 is far smaller than convergence criterion on A_t suggests. This is the consequence of the hierarchical structure of the iterations. The iteration on A_t is at the lowest level, therefore the calculation of A_t is also refined for each EWSB and (times) RGE iteration until the running mass of the A boson and the μ parameter have converged. This leads to a higher precision than naively expected.

4.3 Scan settings

If the algorithm is used in a multidimensional scan of supersymmetric parameters, an example using SuSpect3 is in [71], the m_h MSSM ensures that no spectrum calculation will be performed for parameter sets incompatible with the measured central value of m_h . This leads to a reduction of the parameter space allowed for A_t . However such a calculation, due to the iteration on A_t , has a calculational overhead compared to an MSSM spectrum calculation.

Given that the experimental uncertainty on the m_h measurement is of the order of 0.1 GeV and additionally the theoretical uncertainty is about 2 GeV, the following calculations have been performed with reduced precision: the RGE iterations are stopped when percent level convergence on \bar{m}_A has been reached. All other convergence definitions remain unchanged. These are the standard settings used in Suspect.

To illustrate the calculational overhead the MSSM calculation is compared to the m_h MSSM calculation for s3. The number of RGE iterations is increased from four to six. The algorithm typically adds one additional iteration to each EWSB calculation on top of the three for the stan-

dard algorithm, i.e., a total of 27 iterations is necessary compared to 13 for the standard settings. The calculation of A_t at the first two RGE iterations as a direct calculation of the approximate solution is not computationally intensive. When the fixed point method is used, for the first two RGE iterations, at the first EWSB iteration six and four calculations are necessary to converge on the fixed point to the required accuracy. For the subsequent EWSB iterations typically only one or two iterations on A_t are necessary. For the last two RGE iterations for all EWSB iterations only one or two A_t calculations are necessary. For half of EWSB iterations, a single calculation of A_t is sufficient. The reduction of the number of iterations on A_t as the RGE and EWSB iterations progress illustrates the convergence of the algorithm.

In Table 4 the results on A_t and the calculated m_h are shown for the reduced precision setting of the algorithm. The maximal difference between the calculated Higgs masses is less than 1 MeV, i.e., largely sufficient given the experimental error.

The two EWSB calculations with the μ parameter as input lead to almost identical results for all A_t solutions. The two EWSB calculations with μ use $\bar{m}_{H_u}^2$ as variable to test convergence whereas the other EWSB calculation uses \bar{m}_A^2 to stop the RGE iterations. The calculation is performed with a fixed convergence precision. The impact on the m_h value for a change of $\bar{m}_{H_u}^2$ and \bar{m}_A^2 is not identical. Therefore the results for EWSB with the A boson mass, tree level or pole, can be different with respect to the calculation with the Higgs mass parameters. For the true solution s3, the maximal deviation for all EWSB variants is only two tenth of a permil, at 0.7 GeV with respect to the true A_t of the cliff point 1.

4.4 Beyond the cliff

The cliff point is a favorable situation as four distinct solutions exist. A parameter set can lead to a situation where the local minimum of the Higgs boson mass in the vicinity of $A_t = 0$ GeV is larger than the m_h parameter input. Alternatively the m_h parameter could be higher than either one or both of the maxima of Fig. 1.

To test the validity of the algorithm beyond the proof of concept in the cliff point, the input m_h parameter was varied. The algorithm was slightly extended for m_h values close to the maxima and the local minimum by a bisection algorithm. To ensure a logical coherence of the results, the regions of validity for A_t are defined for the four solutions:

- s1: $-\infty$ to $A_t(m_h^{max}(A_t < 0))$
- s2: $A_t(m_h^{max}(A_t < 0))$ to $A_t(m_h^{min}(A_t \sim 0))$
- s3: $A_t(m_h^{min}(A_t \sim 0))$ to $A_t(m_h^{max}(A_t > 0))$
- s4: $A_t(m_h^{max}(A_t > 0))$ to ∞ .

Table 4 The result of the Higgs inversion algorithm for the three definitions of EWSB input variables is shown. s3 is the true point. The calculated A_t and the resulting m_h are listed for all calculations

EWSB		s1	s2	s3	s4
$m_{H_d}^2, m_{H_u}^2, \text{sign}(\mu)$	A_t [GeV]	-5617.8	-3795.0	3610.5	6085.9
	m_h [GeV]	125.012	125.012	125.012	125.012
$m_A^2(Q), \mu$	A_t [GeV]	-5606.9	-3795.1	3610.7	6090.1
	m_h [GeV]	125.012	125.012	125.012	125.012
m_A, μ	A_t [GeV]	-5607.2	-3794.7	3610.7	6089.9
	m_h [GeV]	125.012	125.012	125.012	125.012

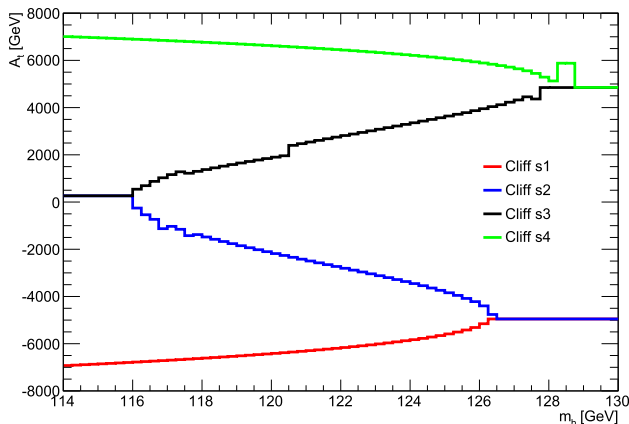


Fig. 4 The result of the determination of A_t is shown as function of the chosen m_h . The determination is performed separately for the four solutions. The histograms are stacked from s1 (bottom) to s4 (top), the horizontal lines at constant A_t at the transition between the regions show only the top color

If the m_h parameter is out of reach, the closest A_t in the region is used.

The result of a scan of m_h values between 112 and 128 GeV is shown in Fig. 4. The four solutions are correctly reconstructed over the full range. For s2 and s3 the lowest parameter values cannot be reached, therefore the A_t value of the local minimal mass is determined. A similar feature is observed when the parameter is greater than the maximal m_h at 2-loop precision shown in Fig. 1. In this case A_t corresponding to the maximal mass achievable for the parameters is determined, resulting in a line parallel to the x-axis. The steps correspond to cases where the μ parameter and the CP-odd scalar Higgs boson mass have converged to a slightly different value which leads to a step in A_t and an offset in the predicted m_h , smaller than the systematic of 2 GeV typically used in scans of the parameter space. In total 256 inversions are shown of which only 3 have not converged correctly. These points are all located in regions where a larger m_h than possible was requested (horizontal lines at $A_t \approx -4.95$ TeV and $A_t \approx 4.85$ TeV) and for two the algorithm returned an error for non convergence. Since the step size of the scan of 0.25 GeV is smaller than the error on the Higgs mass of about 2 GeV, posterior distributions of A_t also give an additional handle on the outliers.

Figure 4 shows A_t as multi-valued function of m_h covering the same parameter space as Fig. 1. This shows that the inversion, based on the exact calculation, works, validating the use of the approximate one-loop calculation as a first guess. However, there could be problematic parameter sets for which the guess points are not sufficiently close to the fixed points to ensure convergence. An alternative algorithm relying on the knowledge of $A_t(m_h^{max}(A_t < 0))$, $A_t(m_h^{min}(A_t \sim 0))$ and $A_t(m_h^{max}(A_t > 0))$, combined with global rather than local criteria, could then be used.

4.5 Beyond the fixed-order approximation

Our inversion strategy is built upon fixed-order diagrammatic results, in particular upon the knowledge of the analytical form of the exact one-loop contribution to the Higgs mass. In more recent developments of MSSM Higgs mass radiative corrections, there are, however, configurations where an EFT approach is better suited for a reliable estimate of the Higgs mass, like typically when considering an MSSM setup with (very) heavy scalars (see e.g. [15] for a recent review). In this case, if for instance a heavy stop sector is integrated out from the low-energy EFT, a direct analytical relation between m_h and A_t will be essentially lost. Nevertheless, an inversion procedure can still be carried out: The needed relation will reside now in the matching condition at the boundary scale between the light and heavy sectors for the quartic Higgs coupling, from which the multi- A_t solutions can be retrieved analytically.

4.6 Beyond the CP-conserving case

If complex phases are allowed for the MSSM parameters, the dependence of m_h on A_t will be in general significantly modified due to loop induced CP-violating mixings among all the neutral Higgs states. The ensuing 3×3 mass matrix after identifying the Goldstone boson, implies an analytical expression of m_h^2 given by a root of a cubic equation, quite different from that obtained from the diagonalization of Eq. (1). Our approach can be easily extended to this case in the (experimentally likely) configuration where the MSSM spectrum,

and in particular the charged Higgs mass, are much heavier than the 125 GeV state. As well known, in this case the CP-violating mixing is essentially confined to the two heavy neutral states sector, see e.g. [72], and the phenomenology (mass, couplings) of the lightest would-be CP-even state becomes essentially the same as in the CP-conserving MSSM. In this limit, taking A_t and μ complex (which is sufficient to account for the physically relevant phases, denoted ϕ_{A_t} and ϕ_μ), the functional dependence of m_h on $|A_t|$ will be the same as that on A_t in the CP-conserving case. The only difference is the reduction of some coefficients by cosine factors, (typically occurrences of $(\mu A_t)^n$ become $(|\mu| |A_t|)^n \cos n(\phi_\mu + \phi_{A_t})$, otherwise even powers A_t^{2n} become $|A_t|^{2n}$, etc.). Modulo these modifications in Eqs. (8) and (18), our algorithm will work exactly as before, to determine $|A_t|$ (and/or $-|A_t|$) solutions from m_h , given ϕ_{A_t} (and or $\phi_{A_t} \pm \pi$), a complex μ , and the other parameters of the MSSM. Beyond this (relative decoupling) limit, the algorithm can still provide an educated guess for $\pm|A_t|$ input, within a more general numerical algorithm for the CP-violating MSSM.

5 Conclusion

The discovery and precise measurement of the Higgs boson motivates the redefinition of the MSSM as m_h MSSM. The algorithm presented in this paper replaces the trilinear coupling of the stop sector A_t with the measured m_h as input parameter.

The simplified expression of the radiative corrections to m_h and the exact full one-loop with the leading two-loop corrections are assembled in an algorithm to calculate A_t . The algorithm has been applied to a benchmark point showing that the four solutions are determined with the expected precision. A single parameter scan with m_h as scan parameter shows that the A_t dependence is correctly reconstructed.

The general structure of the algorithm could also be applied to other parameters. Using the m_h MSSM may speed up the exploration of supersymmetric parameter space by ensuring the compatibility of all calculated spectra with the experimentally measured m_h . Future work will center on applying the algorithm in multi-parameter scans.

Acknowledgements We would like to thank Steve Muanza for his collaboration and input at an early stage of this study, as well as the PESBLADE working group of the OCEVU Labex for useful discussions. We also acknowledge instructive exchanges with Pietro Slavich. This work benefited from partial support of the OCEVU Labex (ANR-11-LABX-0060) and the A*MIDEX project (ANR-11-IDEX-0001-02) funded by the ‘‘Investissements d’ Avenir’’ French government program managed by the ANR.

Data Availability Statement This manuscript has no associated data in a data repository. [Authors’ comment: This is a theoretical study; there are no associated experimental data.]

Open Access This article is licensed under a Creative Commons Attribution 4.0 International License, which permits use, sharing, adaptation, distribution and reproduction in any medium or format, as long as you give appropriate credit to the original author(s) and the source, provide a link to the Creative Commons licence, and indicate if changes were made. The images or other third party material in this article are included in the article’s Creative Commons licence, unless indicated otherwise in a credit line to the material. If material is not included in the article’s Creative Commons licence and your intended use is not permitted by statutory regulation or exceeds the permitted use, you will need to obtain permission directly from the copyright holder. To view a copy of this licence, visit <http://creativecommons.org/licenses/by/4.0/>.

Funded by SCOAP³. SCOAP³ supports the goals of the International Year of Basic Sciences for Sustainable Development.

Appendix A: The coefficients of HiggsMolar(A_t)

We give hereafter the explicit dependence of the coefficients appearing in Eq. (18) on the various $\pi_{ij}^{(\cdot)}$, tadpoles and running mass parameters, as well as the relevant combinations of the latter in terms of the MSSM parameters of the stop sector.

$$\begin{aligned}
 C_0[A_t] &= c_s(\pi_{11}^{(s)} - t_1^{(s)})(\pi_{22}^{(s)} - t_2^{(s)}) \\
 &\quad + (m_h^2 + \pi_{11}^{(0)} - t_1^{(0)} - \bar{m}_{11}^2) \\
 &\quad \cdot (m_h^2 + \pi_{22}^{(0)} - t_2^{(0)} - \bar{m}_{22}^2) - (\pi_{12}^{(0)} - \bar{m}_{12}^2)^2, \\
 C_1[A_t] &= (\pi_{11}^{(s)} - t_1^{(s)})(b_s(\pi_{22}^{(s)} - t_2^{(s)}) - c_s t_2^{(1s)}) \\
 &\quad + (\pi_{22}^{(1)} - t_2^{(1)}) \cdot (m_h^2 + \pi_{11}^{(0)} - t_1^{(0)} - \bar{m}_{11}^2) \\
 &\quad + 2\pi_{12}^{(1)}(\bar{m}_{12}^2 - \pi_{12}^{(0)}), \\
 C_2[A_t] &= (\pi_{11}^{(s)} - t_1^{(s)})(a_s(\pi_{22}^{(s)} - t_2^{(s)}) - b_s t_2^{(1s)}) \\
 &\quad + \pi_{22}^{(2)}(m_h^2 + \pi_{11}^{(0)} - t_1^{(0)} - \bar{m}_{11}^2) - (\pi_{12}^{(1)})^2, \\
 C_3[A_t] &= a_s(t_1^{(s)} - \pi_{11}^{(s)})t_2^{(1s)}, \\
 R_0[A_t] &= (\pi_{11}^{(s)} - t_1^{(s)})(m_h^2 + \pi_{22}^{(0)} - t_2^{(0)} - \bar{m}_{22}^2) \\
 &\quad + (\pi_{22}^{(s)} - t_2^{(s)})(m_h^2 + \pi_{11}^{(0)} - t_1^{(0)} - \bar{m}_{11}^2), \\
 R_1[A_t] &= (t_1^{(s)} - \pi_{11}^{(s)})(t_2^{(1)} - \pi_{22}^{(1)}) \\
 &\quad + (t_1^{(0)} - \pi_{11}^{(0)} + \bar{m}_{11}^2 - m_h^2)t_2^{(1s)}, \\
 R_2[A_t] &= \pi_{22}^{(2)}(\pi_{11}^{(s)} - t_1^{(s)}), \tag{A1}
 \end{aligned}$$

where the \bar{m}_{ij}^2 are given by Eqs. (2)–(4).

Relying on the full one-loop results (and partly on the notations) of [19],⁴ we extract the relevant contributions of the self-energies and tadpoles:

⁴ with, however, an opposite sign convention for μ in accord with Suspect3 [62, 63] and denoting the couplings $\lambda_{s\bar{u}\bar{u}}$ and λ_t of [19] by $g_{s\bar{t}\bar{t}}$ and y_t .

$$16\pi^2(t_1^{(0)} - \pi_{11}^{(0)}) = \frac{3}{\sqrt{2}} \frac{g_2 c_t s_t y_t \mu M^2}{c_\beta M_W} \ln\left(\frac{m_{\tilde{t}_1}}{m_{\tilde{t}_2}}\right) - 3 \sum_{i,j=1}^2 g_{s_1 \tilde{t}_i \tilde{t}_j}^2 B_0(m_{\tilde{t}_i}, m_{\tilde{t}_j}) + \dots, \tag{A2}$$

$$16\pi^2(t_1^{(s)} - \pi_{11}^{(s)}) = \frac{3}{\sqrt{2}} \frac{g_2 c_t s_t y_t \mu}{c_\beta M_W} \left(1 - \ln\left(\frac{m_{\tilde{t}_1} m_{\tilde{t}_2}}{Q^2}\right)\right), \tag{A3}$$

$$16\pi^2(t_2^{(0)} - \pi_{22}^{(0)}) = -3 \left(\sum_{i=1}^2 (\Delta g_i)^2 B_0(m_{\tilde{t}_i}, m_{\tilde{t}_i}) + 2(\Delta g_{12})^2 B_0(m_{\tilde{t}_1}, m_{\tilde{t}_2}) \right) + \dots, \tag{A4}$$

$$16\pi^2(t_2^{(s)} - \pi_{22}^{(s)}) = 0, \tag{A5}$$

$$16\pi^2(t_2^{(1)} - \pi_{22}^{(1)}) = \frac{3}{\sqrt{2}} \frac{g_2 y_t c_t s_t M^2}{s_\beta M_W} \ln\left(\frac{m_{\tilde{t}_2}}{m_{\tilde{t}_1}}\right) - 6\sqrt{2} y_t \left(c_t s_t (\Delta g_1 B_0(m_{\tilde{t}_1}, m_{\tilde{t}_1}) - \Delta g_2 B_0(m_{\tilde{t}_2}, m_{\tilde{t}_2})) + (c_t^2 - s_t^2) \Delta g_{12} B_0(m_{\tilde{t}_1}, m_{\tilde{t}_2}) \right), \tag{A6}$$

$$16\pi^2 t_2^{(1s)} = \frac{3}{\sqrt{2}} \frac{g_2 y_t c_t s_t}{s_\beta M_W} \left(\ln\left(\frac{m_{\tilde{t}_1} m_{\tilde{t}_2}}{Q^2}\right) - 1 \right), \tag{A7}$$

$$16\pi^2 \pi_{22}^{(2)} = 3 y_t^2 \left(2 c_t^2 s_t^2 (B_0(m_{\tilde{t}_1}, m_{\tilde{t}_1}) + B_0(m_{\tilde{t}_2}, m_{\tilde{t}_2})) + (c_t^2 - s_t^2)^2 B_0(m_{\tilde{t}_1}, m_{\tilde{t}_2}) \right), \tag{A8}$$

$$16\pi^2 \pi_{12}^{(0)} = 3 \left(g_{s_1 \tilde{t}_1 \tilde{t}_1} \Delta g_1 B_0(m_{\tilde{t}_1}, m_{\tilde{t}_1}) + g_{s_1 \tilde{t}_2 \tilde{t}_2} \Delta g_2 B_0(m_{\tilde{t}_2}, m_{\tilde{t}_2}) + g_{s_1 \tilde{t}_1 \tilde{t}_2} \Delta g_{12} B_0(m_{\tilde{t}_1}, m_{\tilde{t}_2}) \right) + \dots, \tag{A9}$$

$$16\pi^2 \pi_{12}^{(1)} = \frac{3}{\sqrt{2}} y_t \left(2 c_t s_t (g_{s_1 \tilde{t}_1 \tilde{t}_1} B_0(m_{\tilde{t}_1}, m_{\tilde{t}_1}) - g_{s_1 \tilde{t}_2 \tilde{t}_2} B_0(m_{\tilde{t}_2}, m_{\tilde{t}_2})) + 2(c_t^2 - s_t^2) g_{s_1 \tilde{t}_1 \tilde{t}_2} B_0(m_{\tilde{t}_1}, m_{\tilde{t}_2}) \right) \tag{A10}$$

where we have defined

$$\begin{aligned} \Delta g_1 &\equiv c_t^2 g_{s_2 \tilde{t}_L \tilde{t}_L} + s_t^2 g_{s_2 \tilde{t}_R \tilde{t}_R}, \\ \Delta g_2 &\equiv s_t^2 g_{s_2 \tilde{t}_L \tilde{t}_L} + c_t^2 g_{s_2 \tilde{t}_R \tilde{t}_R}, \\ \Delta g_{12} &\equiv c_t s_t (g_{s_2 \tilde{t}_R \tilde{t}_L} - g_{s_2 \tilde{t}_L \tilde{t}_R}). \end{aligned} \tag{A11}$$

s_β and c_β stand for $\sin \beta$ and $\cos \beta$, and all other quantities have been defined previously, see also Eqs. (14)–(16). The ellipses indicate contributions from the Higgs/Higgsino, gauge/gaugino and other scalar/fermion sectors, that do not have a direct dependence on A_t . The couplings $g_{s_1 \tilde{t}_i \tilde{t}_j}$ are related to $g_{s_1 \tilde{t}_{L,R} \tilde{t}_{L,R}}$, $g_{s_1 \tilde{t}_L \tilde{t}_R}$ as in Eq. (16), but do not depend explicitly on A_t . All parameters appearing in the above expressions are understood to be running in the $\overline{\text{DR}}$ scheme, and Q is the corresponding renormalization scale. The depen-

dence on p^2 , cf. Eq. (1), taken here at $p^2 = m_h^2$, is in the B_0 functions with the shorthand notation $B_0(m_1, m_2) \equiv B_0(m_h, m_1, m_2)$, see also footnote 1.

Note finally that the vanishing of $t_2^{(s)} - \pi_{22}^{(s)}$, cf. Eq. (A5), together with the fact that M^2 appears exclusively with $\ln\left(\frac{m_{\tilde{t}_1}}{m_{\tilde{t}_2}}\right)$, Eqs. (A2) and (A6), and $\sqrt{a_s A_t^2 + b_s A_t + c_s}$ exclusively with $\ln\left(\frac{m_{\tilde{t}_1} m_{\tilde{t}_2}}{Q^2}\right)$, Eqs. (A3) and (A7), are a direct consequence of the cancellation of the quadratic divergences before renormalization as expected in softly-broken SUSY. Indeed, in this case the stop sector contributions from the A_0 function can occur only in the combination $A_0(m_{\tilde{t}_1}) - A_0(m_{\tilde{t}_2})$.

Appendix B: Convergence criterion

A fixed point x_{FP} of a function F , satisfying $F(x_{\text{FP}}) = x_{\text{FP}}$, can be determined iteratively as the limit of a sequence defined by $x_{i+1} = F(x_i)$ and an initial guess x_0 , only if the fixed point is attractive, i.e. $-1 \leq F'(x_{\text{FP}}) \leq 1$. We sketch here how to proceed in the more general cases of non-attractive fixed points:

Define

$$F_\tau(x) = \frac{(\tau - 1)x + F(x)}{\tau}, \quad \text{with } \tau \neq 0, \tag{B.12}$$

and

$$F(x) - F(x_0) = (x - x_0)K(x, x_0) \tag{B.13}$$

with

$$K(x_0, x_0) = F'(x)|_{x=x_0}. \tag{B.14}$$

Let us consider two distinct sequences given by

$$x_{i+1} = F_\tau(x_i) \text{ and } y_{i+1} = F_\tau(y_i), \text{ (with } x_0 \neq y_0), \tag{B.15}$$

and study the variation $F_\tau(x_n) - F_\tau(y_n)$ after n iterations. One finds straightforwardly upon repeated use of Eqs. (B.12), (B.13) and (B.15):

$$\begin{aligned} F_\tau(x_n) - F_\tau(y_n) &= (x_n - y_n) \left(1 + \frac{K(x_n, y_n) - 1}{\tau} \right), \\ &= (F_\tau(x_{n-1}) - F_\tau(y_{n-1})) \left(1 + \frac{K(x_n, y_n) - 1}{\tau} \right), \\ &\vdots \\ F_\tau(x_n) - F_\tau(y_n) &= (x_0 - y_0) \prod_{i=0}^{n-1} \left(1 + \frac{K(x_i, y_i) - 1}{\tau} \right). \end{aligned} \tag{B.16}$$

It follows from Eq. (B.16) that

$$\text{choosing } \tau \text{ such that } \left| 1 + \frac{K(x_i, y_i) - 1}{\tau} \right| \text{ is sufficiently smaller than 1 for a sufficiently large set of } i \text{'s between } 0 \text{ and } n, \quad (\text{B.17})$$

leads to

$$\left| \prod_{i=0}^n \left(1 + \frac{K(x_i, y_i) - 1}{\tau} \right) \right| \ll 1, \quad (\text{B.18})$$

and the two sequences x_i and y_i converge towards each other after n iterations within a prescribed numerical precision. In particular, choosing $y_0 = x_{\text{FP}}$ yields a constant sequence $\{y_i\} = \{x_{\text{FP}}\}$, and x_i converges to the fixed point x_{FP} . This completes the proof that by using the auxiliary function F_τ , one can in principle always optimize the choice of τ depending on the variations of F , so as to converge to x_{FP} for a given initial guess value x_0 , even when dealing with non-attractive fixed points of F . It should be stressed that $K(x_i, y_i)$ is not always a very good estimate of the local variation of F since the two sequences $\{x_i\}$ and $\{y_i\}$ do not necessarily start off close to each other. Nonetheless, it will become so after a few iterations if τ satisfies the criterion (B.17). In particular, for the constant sequence $\{y_i\} \equiv \{x_{\text{FP}}\}$, the successive values of K correspond to variations with respect to the same reference point x_{FP} which is of course not yet known. However, if the initial guess point x_0 is sufficiently close to x_{FP} , one can in practice use $K(x_i, x_{i+1})$ instead of $K(x_i, x_{\text{FP}})$ to optimize τ piece-wise. With this in mind, we can apply the above procedure to the case of L_{FP} , where the quantity $\left(1 + \frac{K(x_i, x_{i+1}) - 1}{\tau} \right)$, with $K(x_i, x_{i+1}) = \Delta L_{\text{FP}} / \Delta x$ being an estimate of $L_{\text{FP}}'(x_{\text{FP}})$ for x_i sufficiently close to x_{FP} , is clearly a discretized version of $L_{\text{FP}}'(x_i)$ as given by Eq. (24). A simple numerical algorithm can thus be devised, based on Eq. (25) as described at the end of Sect. 3.3.

References

- G. Aad et al., Observation of a new particle in the search for the Standard Model Higgs boson with the ATLAS detector at the LHC. Phys. Lett. B **716**, 1–29 (2012). <https://doi.org/10.1016/j.physletb.2012.08.020>. arXiv:1207.7214 [hep-ex]
- S. Chatrchyan et al., Observation of a new boson at a mass of 125 GeV with the CMS experiment at the LHC. Phys. Lett. B **716**, 30–61 (2012). <https://doi.org/10.1016/j.physletb.2012.08.021>. arXiv:1207.7235 [hep-ex]
- S. Chatrchyan et al., Observation of a new boson at a mass of 125 GeV with the CMS experiment at the LHC. Phys. Lett. B **716**, 30–61 (2012). <https://doi.org/10.1016/j.physletb.2012.08.021>. arXiv:1207.7235 [hep-ex]
- A.M. Sirunyan et al., Measurements of properties of the Higgs boson decaying into the four-lepton final state in pp collisions at $\sqrt{s} = 13$ TeV. JHEP **11**, 047 (2017). [https://doi.org/10.1007/JHEP11\(2017\)047](https://doi.org/10.1007/JHEP11(2017)047). arXiv:1706.09936 [hep-ex]
- G. Aad et al., Combined measurement of the Higgs boson mass in pp collisions at $\sqrt{s} = 7$ and 8 TeV with the ATLAS and CMS experiments. Phys. Rev. Lett. **114**, 191803 (2015). <https://doi.org/10.1103/PhysRevLett.114.191803>. arXiv:1503.07589 [hep-ex]
- P.A. Zyla et al., Review of particle physics. PTEP **2020**(8), 083C01 (2020). <https://doi.org/10.1093/ptep/ptaa104>
- S. Schael et al., Precision electroweak measurements on the Z resonance. Phys. Rep. **427**, 257–454 (2006). <https://doi.org/10.1016/j.physrep.2005.12.006>. arXiv:hep-ex/0509008
- I. Dubovyk, A. Freitas, J. Gluza, T. Riemann, J. Usovitsch, Electroweak pseudo-observables and Z-boson form factors at two-loop accuracy. JHEP **08**, 113 (2019). [https://doi.org/10.1007/JHEP08\(2019\)113](https://doi.org/10.1007/JHEP08(2019)113). arXiv:1906.08815 [hep-ph]
- J.-L. Kneur, G. Moultaka, Inverting the supersymmetric standard model spectrum: from physical to Lagrangian gaugino parameters. Phys. Rev. D **59**, 015005 (1999). <https://doi.org/10.1103/PhysRevD.59.015005>. arXiv:hep-ph/9807336
- J.-L. Kneur, G. Moultaka, Phases in the gaugino sector: direct reconstruction of the basic parameters and impact on the neutralino pair production. Phys. Rev. D **61**, 095003 (2000). <https://doi.org/10.1103/PhysRevD.61.095003>. arXiv:hep-ph/9907360
- J.-L. Kneur, N. Sahoury, Bottom-up reconstruction scenarios for (un)constrained MSSM parameters at the LHC. Phys. Rev. D **79**, 075010 (2009). <https://doi.org/10.1103/PhysRevD.79.075010>. arXiv:0808.0144 [hep-ph]
- A. Djouadi, L. Maiani, G. Moreau, A. Polosa, J. Quevillon, V. Riquer, The post-Higgs MSSM scenario: Habemus MSSM? Eur. Phys. J. C **73**, 2650 (2013). <https://doi.org/10.1140/epjc/s10052-013-2650-0>. arXiv:1307.5205 [hep-ph]
- A. Djouadi, The anatomy of electro-weak symmetry breaking. II. The Higgs bosons in the minimal supersymmetric model. Phys. Rep. **459**, 1–241 (2008). <https://doi.org/10.1016/j.physrep.2007.10.005>. arXiv:hep-ph/0503173
- S. Heinemeyer, MSSM Higgs physics at higher orders. Int. J. Mod. Phys. A **21**, 2659–2772 (2006). <https://doi.org/10.1142/S0217751X06031028>. arXiv:hep-ph/0407244
- P. Slavich et al., Higgs-mass predictions in the MSSM and beyond. Eur. Phys. J. C **81**(5), 450 (2021). <https://doi.org/10.1140/epjc/s10052-021-09198-2>. arXiv:2012.15629 [hep-ph]
- P.H. Chankowski, S. Pokorski, J. Rosiek, Charged and neutral supersymmetric Higgs boson masses: complete one loop analysis. Phys. Lett. B **274**, 191–198 (1992). [https://doi.org/10.1016/0370-2693\(92\)90522-6](https://doi.org/10.1016/0370-2693(92)90522-6)
- P.H. Chankowski, S. Pokorski, J. Rosiek, Complete on-shell renormalization scheme for the minimal supersymmetric Higgs sector. Nucl. Phys. B **423**, 437–496 (1994). [https://doi.org/10.1016/0550-3213\(94\)90141-4](https://doi.org/10.1016/0550-3213(94)90141-4). arXiv:hep-ph/9303309
- A. Dabelstein, The one loop renormalization of the MSSM Higgs sector and its application to the neutral scalar Higgs masses. Z. Phys. C **67**, 495–512 (1995). <https://doi.org/10.1007/BF01624592>. arXiv:hep-ph/9409375
- D.M. Pierce, J.A. Bagger, K.T. Matchev, R. Zhang, Precision corrections in the minimal supersymmetric standard model. Nucl. Phys. B **491**, 3–67 (1997). [https://doi.org/10.1016/S0550-3213\(96\)00683-9](https://doi.org/10.1016/S0550-3213(96)00683-9). arXiv:hep-ph/9606211
- R. Hempfling, A.H. Hoang, Two loop radiative corrections to the upper limit of the lightest Higgs boson mass in the minimal supersymmetric model. Phys. Lett. B **331**, 99–106 (1994). [https://doi.org/10.1016/0370-2693\(94\)90948-2](https://doi.org/10.1016/0370-2693(94)90948-2). arXiv:hep-ph/9401219
- S. Heinemeyer, W. Hollik, G. Weiglein, QCD corrections to the masses of the neutral CP-even Higgs bosons in the MSSM. Phys. Rev. D **58**, 091701 (1998). <https://doi.org/10.1103/PhysRevD.58.091701>. arXiv:hep-ph/9803277

22. S. Heinemeyer, W. Hollik, G. Weiglein, The masses of the neutral CP-even Higgs bosons in the MSSM: accurate analysis at the two loop level. *Eur. Phys. J. C* **9**, 343–366 (1999). <https://doi.org/10.1007/s100529900006>. arXiv:hep-ph/9812472
23. S. Heinemeyer, W. Hollik, G. Weiglein, Precise prediction for the mass of the lightest Higgs boson in the MSSM. *Phys. Lett. B* **440**, 296–304 (1998). [https://doi.org/10.1016/S0370-2693\(98\)01116-2](https://doi.org/10.1016/S0370-2693(98)01116-2). arXiv:hep-ph/9807423
24. S. Heinemeyer, W. Hollik, H. Rzehak, G. Weiglein, High-precision predictions for the MSSM Higgs sector at $O(\alpha(b)\alpha(s))$. *Eur. Phys. J. C* **39**, 465–481 (2005). <https://doi.org/10.1140/epjc/s2005-02112-6>. arXiv:hep-ph/0411114
25. R.-J. Zhang, Two loop effective potential calculation of the lightest CP even Higgs boson mass in the MSSM. *Phys. Lett. B* **447**, 89–97 (1999). [https://doi.org/10.1016/S0370-2693\(98\)01575-5](https://doi.org/10.1016/S0370-2693(98)01575-5). arXiv:hep-ph/9808299
26. J.R. Espinosa, R.-J. Zhang, MSSM lightest CP even Higgs boson mass to $O(\alpha(s)\alpha(t))$: The Effective potential approach. *JHEP* **03**, 026 (2000). <https://doi.org/10.1088/1126-6708/2000/03/026>. arXiv:hep-ph/9912236
27. J.R. Espinosa, R.-J. Zhang, Complete two loop dominant corrections to the mass of the lightest CP even Higgs boson in the minimal supersymmetric standard model. *Nucl. Phys. B* **586**, 3–38 (2000). [https://doi.org/10.1016/S0550-3213\(00\)00421-1](https://doi.org/10.1016/S0550-3213(00)00421-1). arXiv:hep-ph/0003246
28. G. Degrassi, P. Slavich, F. Zwirner, On the neutral Higgs boson masses in the MSSM for arbitrary stop mixing. *Nucl. Phys. B* **611**, 403–422 (2001). [https://doi.org/10.1016/S0550-3213\(01\)00343-1](https://doi.org/10.1016/S0550-3213(01)00343-1). arXiv:hep-ph/0105096
29. A. Brignole, G. Degrassi, P. Slavich, F. Zwirner, On the $O(\alpha(t)^2)$ two loop corrections to the neutral Higgs boson masses in the MSSM. *Nucl. Phys. B* **631**, 195–218 (2002). [https://doi.org/10.1016/S0550-3213\(02\)00184-0](https://doi.org/10.1016/S0550-3213(02)00184-0). arXiv:hep-ph/0112177
30. A. Brignole, G. Degrassi, P. Slavich, F. Zwirner, On the two loop sbottom corrections to the neutral Higgs boson masses in the MSSM. *Nucl. Phys. B* **643**, 79–92 (2002). [https://doi.org/10.1016/S0550-3213\(02\)00748-4](https://doi.org/10.1016/S0550-3213(02)00748-4). arXiv:hep-ph/0206101
31. A. Dedes, P. Slavich, Two loop corrections to radiative electroweak symmetry breaking in the MSSM. *Nucl. Phys. B* **657**, 333–354 (2003). [https://doi.org/10.1016/S0550-3213\(03\)00173-1](https://doi.org/10.1016/S0550-3213(03)00173-1). arXiv:hep-ph/0212132
32. A. Dedes, G. Degrassi, P. Slavich, On the two loop Yukawa corrections to the MSSM Higgs boson masses at large $\tan\beta$. *Nucl. Phys. B* **672**, 144–162 (2003). <https://doi.org/10.1016/j.nuclphysb.2003.08.033>. arXiv:hep-ph/0305127
33. G. Degrassi, S. Heinemeyer, W. Hollik, P. Slavich, G. Weiglein, Towards high precision predictions for the MSSM Higgs sector. *Eur. Phys. J. C* **28**, 133–143 (2003). <https://doi.org/10.1140/epjc/s2003-01152-2>. arXiv:hep-ph/0212020
34. S.P. Martin, Complete two loop effective potential approximation to the lightest Higgs scalar boson mass in supersymmetry. *Phys. Rev. D* **67**, 095012 (2003). <https://doi.org/10.1103/PhysRevD.67.095012>. arXiv:hep-ph/0211366
35. S.P. Martin, Strong and Yukawa two-loop contributions to Higgs scalar boson self-energies and pole masses in supersymmetry. *Phys. Rev. D* **71**, 016012 (2005). <https://doi.org/10.1103/PhysRevD.71.016012>. arXiv:hep-ph/0405022
36. S. Borowka, T. Hahn, S. Heinemeyer, G. Heinrich, W. Hollik, Momentum-dependent two-loop QCD corrections to the neutral Higgs-boson masses in the MSSM. *Eur. Phys. J. C* **74**(8), 2994 (2014). <https://doi.org/10.1140/epjc/s10052-014-2994-0>. arXiv:1404.7074 [hep-ph]
37. G. Degrassi, S. Di Vita, P. Slavich, Two-loop QCD corrections to the MSSM Higgs masses beyond the effective-potential approximation. *Eur. Phys. J. C* **75**(2), 61 (2015). <https://doi.org/10.1140/epjc/s10052-015-3280-5>. arXiv:1410.3432 [hep-ph]
38. S.P. Martin, Three-loop corrections to the lightest Higgs scalar boson mass in supersymmetry. *Phys. Rev. D* **75**, 055005 (2007). <https://doi.org/10.1103/PhysRevD.75.055005>. arXiv:hep-ph/0701051
39. R.V. Harlander, P. Kant, L. Mihaila, M. Steinhauser, Higgs boson mass in supersymmetry to three loops. *Phys. Rev. Lett.* **100**, 191602 (2008). <https://doi.org/10.1103/PhysRevLett.101.039901>. arXiv:0803.0672 [hep-ph]
40. P. Kant, R.V. Harlander, L. Mihaila, M. Steinhauser, Light MSSM Higgs boson mass to three-loop accuracy. *JHEP* **08**, 104 (2010). [https://doi.org/10.1007/JHEP08\(2010\)104](https://doi.org/10.1007/JHEP08(2010)104). arXiv:1005.5709 [hep-ph]
41. R.V. Harlander, J. Klappert, A. Voigt, Higgs mass prediction in the MSSM at three-loop level in a pure $\overline{\text{DR}}$ context. *Eur. Phys. J. C* **77**(12), 814 (2017). <https://doi.org/10.1140/epjc/s10052-017-5368-6>. arXiv:1708.05720 [hep-ph]
42. J.A. Aguilar-Saavedra et al., Supersymmetry parameter analysis: SPA convention and project. *Eur. Phys. J. C* **46**, 43–60 (2006). <https://doi.org/10.1140/epjc/s2005-02460-1>. arXiv:hep-ph/0511344
43. G. Aad et al., Search for squarks and gluinos in final states with jets and missing transverse momentum using 139 fb⁻¹ of $\sqrt{s} = 13$ TeV pp collision data with the ATLAS detector. *JHEP* **02**, 143 (2021). [https://doi.org/10.1007/JHEP02\(2021\)143](https://doi.org/10.1007/JHEP02(2021)143). arXiv:2010.14293 [hep-ex]
44. G. Aad et al., Search for electroweak production of charginos and sleptons decaying into final states with two leptons and missing transverse momentum in $\sqrt{s} = 13$ TeV pp collisions using the ATLAS detector. *Eur. Phys. J. C* **80**(2), 123 (2020). <https://doi.org/10.1140/epjc/s10052-019-7594-6>. arXiv:1908.08215 [hep-ex]
45. A.M. Sirunyan et al., Search for supersymmetry in proton-proton collisions at 13 TeV in final states with jets and missing transverse momentum. *JHEP* **10**, 244 (2019). [https://doi.org/10.1007/JHEP10\(2019\)244](https://doi.org/10.1007/JHEP10(2019)244). arXiv:1908.04722 [hep-ex]
46. A. Tumasyan et al., Search for electroweak production of charginos and neutralinos in proton–proton collisions at $\sqrt{s} = 13$ TeV. *JHEP* **04**, 147 (2022). arXiv:2106.14246 [hep-ex]
47. A.M. Sirunyan et al., Search for supersymmetry in final states with two oppositely charged same-flavor leptons and missing transverse momentum in proton–proton collisions at $\sqrt{s} = 13$ TeV. *JHEP* **04**, 123 (2021). [https://doi.org/10.1007/JHEP04\(2021\)123](https://doi.org/10.1007/JHEP04(2021)123). arXiv:2012.08600 [hep-ex]
48. G. Aad et al., Search for a scalar partner of the top quark in the all-hadronic $t\bar{t}$ plus missing transverse momentum final state at $\sqrt{s} = 13$ TeV with the ATLAS detector. *Eur. Phys. J. C* **80**(8), 737 (2020). <https://doi.org/10.1140/epjc/s10052-020-8102-8>. arXiv:2004.14060 [hep-ex]
49. A.M. Sirunyan et al., Search for top squark production in fully-hadronic final states in proton–proton collisions at $\sqrt{s} = 13$ TeV. *Phys. Rev. D* **104**(5), 052001 (2021). <https://doi.org/10.1103/PhysRevD.104.052001>. arXiv:2103.01290 [hep-ex]
50. J.R. Ellis, G. Ridolfi, F. Zwirner, Radiative corrections to the masses of supersymmetric Higgs bosons. *Phys. Lett. B* **257**, 83–91 (1991). [https://doi.org/10.1016/0370-2693\(91\)90863-L](https://doi.org/10.1016/0370-2693(91)90863-L)
51. H.E. Haber, R. Hempfling, Can the mass of the lightest Higgs boson of the minimal supersymmetric model be larger than $m(Z)$? *Phys. Rev. Lett.* **66**, 1815–1818 (1991). <https://doi.org/10.1103/PhysRevLett.66.1815>
52. Y. Okada, M. Yamaguchi, T. Yanagida, Renormalization group analysis on the Higgs mass in the softly broken supersymmetric standard model. *Phys. Lett. B* **262**, 54–58 (1991). [https://doi.org/10.1016/0370-2693\(91\)90642-4](https://doi.org/10.1016/0370-2693(91)90642-4)
53. M. Carena, J.R. Espinosa, M. Quiros, C.E.M. Wagner, Analytical expressions for radiatively corrected Higgs masses and couplings in the MSSM. *Phys. Lett. B* **355**, 209–221 (1995). [https://doi.org/10.1016/0370-2693\(95\)00694-G](https://doi.org/10.1016/0370-2693(95)00694-G). arXiv:hep-ph/9504316

54. M. Carena, M. Quiros, C.E.M. Wagner, Effective potential methods and the Higgs mass spectrum in the MSSM. *Nucl. Phys. B* **461**, 407–436 (1996). [https://doi.org/10.1016/0550-3213\(95\)00665-6](https://doi.org/10.1016/0550-3213(95)00665-6). arXiv:hep-ph/9508343
55. H.E. Haber, R. Hempfling, A.H. Hoang, Approximating the radiatively corrected Higgs mass in the minimal supersymmetric model. *Z. Phys. C* **75**, 539–554 (1997). <https://doi.org/10.1007/s002880050498>. arXiv:hep-ph/9609331
56. M. Carena, H.E. Haber, S. Heinemeyer, W. Hollik, C.E.M. Wagner, G. Weiglein, Reconciling the two loop diagrammatic and effective field theory computations of the mass of the lightest CP-even Higgs boson in the MSSM. *Nucl. Phys. B* **580**, 29–57 (2000). [https://doi.org/10.1016/S0550-3213\(00\)00212-1](https://doi.org/10.1016/S0550-3213(00)00212-1). arXiv:hep-ph/0001002
57. S. Heinemeyer, W. Hollik, G. Weiglein, FeynHiggsFast: a Program for a fast calculation of masses and mixing angles in the Higgs sector of the MSSM (2000). arXiv:hep-ph/0002213
58. P.Z. Skands et al., SUSY Les Houches accord: interfacing SUSY spectrum calculators, decay packages, and event generators. *JHEP* **07**, 036 (2004). <https://doi.org/10.1088/1126-6708/2004/07/036>. arXiv:hep-ph/0311123
59. B.C. Allanach, A. Djouadi, J.L. Kneur, W. Porod, P. Slavich, Precise determination of the neutral Higgs boson masses in the MSSM. *JHEP* **09**, 044 (2004). <https://doi.org/10.1088/1126-6708/2004/09/044>. arXiv:hep-ph/0406166
60. B.C. Allanach, A. Voigt, Uncertainties in the lightest CP even Higgs boson mass prediction in the minimal supersymmetric standard model: fixed order versus effective field theory prediction. *Eur. Phys. J. C* **78**(7), 573 (2018). <https://doi.org/10.1140/epjc/s10052-018-6046-z>. arXiv:1804.09410 [hep-ph]
61. H. Bahl, S. Heinemeyer, W. Hollik, G. Weiglein, Theoretical uncertainties in the MSSM Higgs boson mass calculation. *Eur. Phys. J. C* **80**(6), 497 (2020). <https://doi.org/10.1140/epjc/s10052-020-8079-3>. arXiv:1912.04199 [hep-ph]
62. A. Djouadi, J.L. Kneur, G. Moultaka, SuSpect: a Fortran code for the supersymmetric and Higgs particle spectrum in the MSSM. *Comput. Phys. Commun.* **176**, 426–455 (2007). <https://doi.org/10.1016/j.cpc.2006.11.009>. arXiv:hep-ph/0211331
63. G. Brooijmans et al., Les Houches 2011: physics at TeV colliders new physics working group report, in *7th Les Houches Workshop on Physics at TeV Colliders* (2012), pp. 221–463. arXiv:1203.1488 [hep-ph]
64. B.C. Allanach, SOFTSUSY: a program for calculating supersymmetric spectra. *Comput. Phys. Commun.* **143**, 305–331 (2002). [https://doi.org/10.1016/S0010-4655\(01\)00460-X](https://doi.org/10.1016/S0010-4655(01)00460-X). arXiv:hep-ph/0104145
65. W. Porod, SPheno, a program for calculating supersymmetric spectra, SUSY particle decays and SUSY particle production at e^+e^- colliders. *Comput. Phys. Commun.* **153**, 275–315 (2003). [https://doi.org/10.1016/S0010-4655\(03\)00222-4](https://doi.org/10.1016/S0010-4655(03)00222-4). arXiv:hep-ph/0301101
66. W. Porod, F. Staub, SPheno 3.1: extensions including flavour, CP-phases and models beyond the MSSM. *Comput. Phys. Commun.* **183**, 2458–2469 (2012). <https://doi.org/10.1016/j.cpc.2012.05.021>. arXiv:1104.1573 [hep-ph]
67. F. Staub, W. Porod, Improved predictions for intermediate and heavy Supersymmetry in the MSSM and beyond. *Eur. Phys. J. C* **77**(5), 338 (2017). <https://doi.org/10.1140/epjc/s10052-017-4893-7>. arXiv:1703.03267 [hep-ph]
68. S. Heinemeyer, W. Hollik, G. Weiglein, FeynHiggs: a Program for the calculation of the masses of the neutral CP even Higgs bosons in the MSSM. *Comput. Phys. Commun.* **124**, 76–89 (2000). [https://doi.org/10.1016/S0010-4655\(99\)00364-1](https://doi.org/10.1016/S0010-4655(99)00364-1). arXiv:hep-ph/9812320
69. H. Bahl, T. Hahn, S. Heinemeyer, W. Hollik, S. Paßehr, H. Rzehak, G. Weiglein, Precision calculations in the MSSM Higgs-boson sector with FeynHiggs 2.14. *Comput. Phys. Commun.* **249**, 107099 (2020). <https://doi.org/10.1016/j.cpc.2019.107099>. arXiv:1811.09073 [hep-ph]
70. P. Athron, J.H. Park, D. Stöckinger, A. Voigt, FlexibleSUSY—a spectrum generator for supersymmetric models. *Comput. Phys. Commun.* **190**, 139–172 (2015). <https://doi.org/10.1016/j.cpc.2014.12.020>. arXiv:1406.2319 [hep-ph]
71. A. Butter, T. Plehn, M. Rauch, D. Zerwas, S. Henrot-Versillé, R. Lafaye, Invisible Higgs decays to Hooperons in the NMSSM. *Phys. Rev. D* **93**, 015011 (2016). <https://doi.org/10.1103/PhysRevD.93.015011>. arXiv:1507.02288 [hep-ph]
72. A. Pilaftsis, C.E.M. Wagner, Higgs bosons in the minimal supersymmetric standard model with explicit CP violation. *Nucl. Phys. B* **553**(1–2), 3–42 (1999). [https://doi.org/10.1016/S0550-3213\(99\)00261-8](https://doi.org/10.1016/S0550-3213(99)00261-8)